Hydrodynamical simulations of the Lyα forest: data comparisons

Avery Meiksin[1], Greg Bryan[2,3], Marie Machacek[2,4]
[1] *Institute for Astronomy, University of Edinburgh, Blackford Hill, Edinburgh EH9 3HJ, UK*
[2] *Department of Physics, MIT, 77 Massachusetts Avenue, Cambridge, MA 02139 , USA*
[3] *Hubble Fellow*
[4] *On leave from Department of Physics, Northeastern University, Boston, MA, USA*

1 February 2008

ABSTRACT
Numerical hydrodynamical simulations are used to predict the expected absorption properties of the Lyα forest for a variety of Cold Dark Matter dominated cosmological scenarios: CHDM, OCDM, ΛCDM, SCDM, and tCDM. Synthetic spectra are constructed duplicating the resolution, signal-to-noise ratio, and wavelength coverage of several published high resolution spectra, and their statistical properties compared on the basis of the flux distribution of the spectra, the distribution of coefficients in a wavelet decomposition of the spectra, and the distributions of absorption line profile parameters. Agreement between the measured and predicted cumulative distributions is found at the few to several percent level. The best-fitting models to the flux distribution correspond to normalizations on the scale of the cosmological Jeans length of $1.3 < \sigma_{\rm J} < 1.7$ at $z = 3$. No single model provides a statistically acceptable match to all the distributions. Significantly larger median Doppler parameters are found in the measured spectra than predicted by all but the lowest normalization models (CHDM and tCDM), which provide poor fits to the flux distributions. The discrepancy in Doppler parameters is particularly large for absorption systems optically thin at the Lyα line-centre. This may indicate a need to introduce additional energy injection throughout the intergalactic medium, as may be provided by late He II reionization ($z_{\rm HeII} \simeq 3.5$) or supernovae-driven winds from young galaxies, and/or a larger baryon fraction than given by recent determinations of the deuterium abundance within the context of standard Big Bang Nucleosynthesis. The models require a hydrogen ionization rate at redshifts $1.7 < z < 3.8$ within a factor of 2 of that predicted from QSOs alone as the sources of the UV photoionization background, although with a slower rate of decline with redshift at $z > 3.5$ than predicted from current QSO counts. Principal systematic uncertainties in comparing the models with the observations are the setting of the continuum level of the QSO spectra and the prevalence of metal absorption lines, particularly at $z < 3$.

Key words: hydrodynamics – methods: numerical – intergalactic medium – quasars: absorption lines – cosmology: theory – large-scale structure of Universe

1 INTRODUCTION

The successful recovery of the observed statistical properties of the Lyα forest by numerical simulations in the context of various cold dark matter (CDM) dominated cosmologies suggests that the gravitational instability scenario provides a broadly accurate description of the development and evolution of the structure of the intergalactic medium (IGM) (Cen et al. 1994; Zhang, Anninos, & Norman 1995; Hernquist et al. 1996; Zhang et al. 1997; Bond & Wadsley 1997; Theuns, Leonard & Efstathiou 1998a). The simulations show that nearly the entire IGM fragments into filaments, sheets, and fluctuations in underdense minivoids, all of which give rise to the absorption lines comprising the Lyα forest detected in the spectra of Quasi-Stellar Objects (QSOs) (Cen et al. 1994; Miralda-Escudè et al. 1996; Zhang et al. 1998). By analysing synthetic spectra drawn from the simulations, it has been demonstrated that the measured flux distributions, neutral hydrogen column density distributions, and the evolution in the number of absorption lines per unit redshift are reasonably well accounted for by the complex web of interconnecting structures found in the simulations.

The structure of the Lyα forest is intermediate in complexity between that of the Cosmic Microwave Background (CMB) and the large-scale distribution of galaxies. It may be reasonably hoped that the physics of gravitational instability and hydrodynamics alone, once a model for the reionization of the IGM is assumed, is adequate for describing the measurements of the Lyα forest. In this sense, the Lyα forest represents a bridge between the relatively straightforward mechanisms believed responsible for the formation of the CMB fluctuations (given an input cosmological model and linear power spectrum), and the complex physical processes involved in galaxy formation. For this reason, the Lyα forest offers a unique forum for testing models of structure formation.

The Keck HIRES (Hu et al. 1995; Lu et al. 1996; Kirkman & Tytler 1997) and, more recently, the VLT UVES (Cristiani & D'Odorico 2000) have provided high resolution (6–9 $\mathrm{km\,s^{-1}}$), high signal-to-noise ratio (50–100 per pixel) observations of the Lyα forest that resolve the structure of the absorption features, and have dramatically improved the precision with which model predictions may be compared with the measured statistical properties of the Lyα forest. The high precision of the data has elicited similar precision in the predictions from numerical simulations. Comparisons between the model predictions and the observations have been effected by several groups by using the simulation results to synthesize spectra that mimic the pixelization and typical noise characteristics of the measured spectra. Adopting this approach, Davé et al. (1997) compare the predictions of their standard CDM (SCDM) simulation for the distributions of H I column densities and Doppler parameters, as derived from Voigt profile absorption line fitting to synthesized spectra, with the distributions reported by Hu et al. (1995); Rauch et al. (1997) compare the predictions of an SCDM model and a flat CDM model with a non-vanishing cosmological constant (ΛCDM) for the distribution of pixel fluxes with distributions measured from several Keck HIRES QSO spectra; Theuns et al. (1998b, 1999) compare the predictions of an open CDM (OCDM), SCDM, and ΛCDM simulations for the distributions of absorption line parameters with those reported by Hu et al. (1995), Lu et al. (1996), and Kim et al. (1997); Weinberg et al. (1999) provide a preliminary low-resolution comparison between the predicted flux per pixel distributions of several cosmological models with that measured in a sample of Keck HIRES spectra; and McDonald et al. (2000b) compare the prediction of the ΛCDM simulation of Miralda-Escudé et al. (1996) for the distribution of pixel fluxes with the measured distribution averaged over several HIRES QSO spectra. (In addition to mimicking the pixelization of the HIRES, Rauch et al. 1997, Theuns et al. 1998b and McDonald et al. 2000b also incorporate the effect of the spectral resolution of the HIRES in their synthetic spectra.) Because of the required small box sizes of the simulations, the synthetic spectra are much shorter than those measured, which cover a fairly broad range in redshift (typically $\Delta z \approx 0.5$). This limitation has necessitated several approaches that degrade the precision of the comparison between the simulation predictions and the data: assuming that an average distribution measured over a range of redshifts is the same as the distribution at the average redshift (Davé et al. 1997; Theuns et al. 1998b, 1999; McDonald et al. 2000; Machacek et al. 2000); correcting the measured optical depths according to an assumed evolutionary rule (Rauch et al. 1997, who assumed the pixel optical depths scale as $\tau(z) \propto (1+z)^{4.5}$); or comparing the predicted and measured distributions over broad redshift bins (McDonald et al. 2000).

In addition to the tests above, there has been a parallel effort to compare the predictions of the simulations for the flux power spectrum (Croft et al. 2000 and references therein; McDonald et al. 2000b) and auto- and cross-correlation functions (Zuo & Bond 1994; Miralda-Escudé et al. 1996; McDonald et al. 2000b) with the observations. These approaches target the measurement of large-scale clustering (low k) properties of the IGM and, implicitly, of the underlying dark matter, more than the smaller scale (high k) absorption properties of the Lyα forest (although the two are related), as a means for constraining models of large-scale structure formation. In this paper we concentrate on the smaller scale properties of the IGM and make no further mention of these complementary statistics.

The comparisons between the simulations and data on the basis of the flux and H I column density distributions have consistently produced very good agreement. An outstanding difficulty is the somewhat poorer agreement found for the distribution of Doppler parameters. The simulation convergence tests of Theuns et al. (1998b) and Bryan et al. (1999) show that as the resolution of the simulations increases, the absorption lines tend to narrow, although the trend need not be strictly monotonic (Meiksin & White 2001). As a consequence, the SCDM, OCDM and ΛCDM simulations predict smaller Doppler parameters than measured (at least when restricted to $N_{\rm HI} > 10^{13}\,\mathrm{cm^{-2}}$ systems), without the introduction of additional heating of the IGM (Theuns et al. 1999; Bryan & Machacek 2000; Machacek et al. 2000; Theuns, Schaye & Haehnelt 2000). The improved agreement found by Machacek et al. (2000) between the predictions of a tilted CDM (tCDM) model and the distribution of Doppler parameters reported by Kim et al. (1997), however, suggests that the case for disagreement may depend on the assumed cosmological model.

While the concordance between the simulation predictions and measurements of the Lyα forest has been good, statistical quantifications of the level of agreement have generally been absent, rendering it difficult to assess the importance of discrepancies, as in the Doppler parameter distributions. It also leaves open the more general question: are the predictions of the numerical simulations consistent with the observations at a statistically acceptable level? It is a central goal of this paper to address this question. Progress toward an answer has recently been made by McDonald et al. (2000b), who quantify the agreement between the pixel flux distribution for a ΛCDM simulation and the mean measured distribution based on several HIRES spectra. To do so, however, they split the flux values into several (21) bins and use the χ^2 statistic as a basis for comparison, finding agreement between the simulated and measured distributions for $z > 3$, but not at $z = 2.41$. Given the high resolution and wide wavelength range of the spectra, a far greater number of degrees-of-freedom are available, permitting more stringent tests. For a typical pixel number of $N \approx 10^4$, it should be possible to measure the cumulative flux distribution to a precision of $1/N^{1/2} \approx 0.01$, or perhaps a few times this allowing for correlations in the flux values of neighbouring

pixels. No group has fully exploited the information available from Voigt profile fitting, which typically produces several hundred lines per spectrum.

A principal theme of this paper is to determine how closely the simulation predictions match the statistics of the Lyα forest, as extracted directly from the measured spectra, and to determine the limitations involved, both observational and theoretical. To do so, we use a suite of simulations for a variety of cosmological models to construct synthetic spectra designed to match the resolution, pixelization, wavelength coverage, and noise properties of a set of measured spectra published in the literature. Both the synthesized and measured spectra are analysed using identical software to minimize any differences due to the arbitrary nature of the algorithms. In this way, we are able to determine how sensitive the statistics of the absorption features are to the properties of the spectra, including data-reduction systematics, like the uncertainty in the continuum-fitting. We employ several statistical tools: the distribution of flux per pixel, the distributions of H I column density and Doppler parameters, and a novel approach based on the Discrete Wavelet Transform (DWT) of the data (Meiksin 2000).

This paper differs from previous work in several important regards: 1. We simulate the full wavelength coverage of the measured spectra (between Lyα and Lyβ), to the wavelength precision of the spectra, incorporating the specific noise characteristics of each spectrum. 2. We consider a broader range of statistical tests, and employ identical software to analyse both the simulations and the measured spectra. 3. We introduce statistical quantifications of the differences between the model predictions and the observations, including analyses of the probability distributions of the tests employed. 4. We consider a broader range of cosmological models than has been done previously in the context of the full set of tests considered. 5. Lastly, our fluid computational method differs fundamentally from those employed in most of the other simulations. While most use Smoothed Particle Hydrodynamics (SPH) with artificial viscosity to solve for the hydrodynamics part of the simulations, we use an Eulerian (in the co-moving frame) finite-difference shock-capturing scheme employing the Piecewise Parabolic Method (PPM). The exception is the ΛCDM model of Miralda-Escudé et al. (1996), who also used an Eulerian shock-capturing scheme, based on the total variation diminishing scheme. We believe it important to consider simulations using different numerical schemes, particularly when making high precision comparisons with the data.

Our ultimate goal, toward which this paper is directed, is to determine whether or not the data and the simulations are of adequate accuracy to distinguish between differing cosmological models and reionization scenarios. If so, the simulations should provide a valuable independent tool for testing models of structure formation as well as probing the physical state of the gas and the energetic processes that accompanied the formation of early sources of photoionization, whether QSOs, galaxies, or smaller stellar systems.

The paper is organized as follows. In the next section we describe the methods used to compare the simulation results with the measured spectra. In §III, the analysis results for seven QSO spectra are presented. A discussion of the results follows in §IV. Our conclusions are summarised in §V. Various tests of the analysis procedures and absorption line fitting algorithms are presented in the two appendices.

2 ANALYSIS METHODS

2.1 Models and spectra

The models used in the paper are described in detail in Machacek et al. (2000) (M00) and summarised in Table 1. All the models considered are in the context of CDM dominated cosmologies. The following six models were simulated using Kronos (Bryan et al. 1995), a combined Particle Mesh (PM) + PPM gravity-hydrodynamics code: a standard critical-density flat CDM model (SCDM), two flat CDM models with a non-vanishing cosmological constant and low (ΛCDM$_{\rm L}$) and high (ΛCDM$_{\rm H}$) baryon densities, an open CDM model (OCDM), a tilted flat CDM model (tCDM), and a flat critical-density mixed dark matter model with a hot component added to the CDM (CHDM). All the power spectra have been normalized to be consistent with the abundances of rich clusters (White, Efstathiou & Frenk 1993; Bond & Myers 1996; Eke, Coles & Frenk 1996; Pierpaoli, Scott & White 2000), as the scales involved are near the scales relevant to the formation of the structures giving rise to the Lyα forest. In addition, the tilt adopted in the tCDM model was chosen also to match the normalization on large scales (although only marginally) as determined from the COBE measurements of the CMB (Bunn & White 1997). The ΛCDM$_{\rm H}$ model was designed to yield larger Doppler parameters than the ΛCDM$_{\rm L}$ model in an attempt to better match the measured values. Accordingly, in addition to increasing the baryon density, we have boosted the rate of He II heating by QSO sources by a factor of 1.8 to mimic the sudden onset of He II photoionization at late times (Bryan & Machacek 2000). There is some uncertainty as to the best value of the baryon density $\Omega_b h^2$ to adopt, as there is some spread depending on the method by which it is measured. Measurements based on deuterium abundances within the context of standard Big Bang Nucleosynthesis (BBN) (Burles & Tytler 1998; O'Meara et al. 2000) yield lower values than the best estimates based on measurements of the acoustic peaks in the CMB (Netterfield et al. 2001; Pryke et al. 2001; Stompor et al. 2001). The values adopted for all the models are consistent with the limits of Copi, Schramm & Turner (1995) based on a variety of observational constraints. The value used for the ΛCDM$_{\rm L}$, OCDM and SCDM models is at the 3σ lower limit of Burles & Tytler (1998) and O'Meara et al. (2000) based on measurements of the deuterium abundances in intergalactic gas clouds, and assuming no destruction of primordial deuterium. (Absorption systems with low metallicity were specifically chosen by these groups to ensure the effects of stellar processing were minimal, but a small amount of processing would in principle permit a lower value for $\Omega_b h^2$.) The value for the ΛCDM$_{\rm H}$ model agrees with the best estimate of O'Meara et al. (2000) and Pryke et al. (2001). The value used for the CHDM and tCDM models is midway between the best estimates of O'Meara et al. (2000) and Stompor et al. (2001).

The initial data for all models except the CHDM and ΛCDM$_{\rm H}$ models were generated using COSMICS (Bertschinger 1995) with the BBKS transfer function

(Bardeen et al. 1986) to compute the starting redshifts and the unconstrained initial particle positions and velocity perturbations appropriate for each model. For the CHDM model we used CMBFAST (Seljak & Zaldarriaga 1996) to generate the initial conditions. For the ΛCDM$_{\rm H}$ model the power spectrum was based on the analytic fits of Eisenstein & Hu (1999).

We use the synthetic spectra described in M00. The spectra are resampled according to the pixelizations given in Table 2, and the spectral resolution mimicked by smoothing the spectra with a gaussian of the indicated widths. Noise was added according to the varying signal-to-noise ratio across each measured spectrum, as described below.

In order to construct spectra with the identical wavelength coverage as the observed spectra, the simulation results from a broad range in redshifts must be used. Since the simulation results are saved at only integral redshift values between $z = 1$ and $z = 5$ (except for the ΛCDM$_{\rm H}$ model, for which the data are saved more frequently), it is necessary to interpolate between redshifts. (We do not use the $z = 1$ results since the fundamental mode across the simulation volume has grown too large by this time to be certain of the reliability of the results.) To assist in the interpolation, we take advantage of the redshift scaling relations of the gas properties found by M00. Because the gas is in photoionisation equilibrium, the optical depth at any given wavelength scales like $\tau(\lambda) \propto n^2\alpha_A(T)/[\Gamma(z)H(z)]$, where n is the gas density, $\alpha_A(T)$ is the (Case A) radiative recombination coefficient at gas temperature T, $H(z)$ is the Hubble constant at redshift z, and $\Gamma(z)$ is the incident rate of ionising photons per neutral atom. Since the morphologies and overdensities of the overdense structures evolve only slowly in the comoving frame and T scales like the square-root of the gas overdensity (Zhang et al. 1998), and since $\alpha_A(T) \propto T^{-0.7}$ (approximately), we may expect the combination $n^2\alpha_A(T)$ to scale like a power of the mean gas density $\bar{n}(z)$, which itself scales as $(1+z)^3$. Accordingly, we scale the optical depths according to $\tau(z) \propto (1+z)^\alpha/[\Gamma(z)H(z)]$. The value $\alpha = 6$ is expected for a homogeneously expanding medium of fixed temperature. We find that in general α is model-dependent. For any particular cosmological model, we determine α between two redshifts z_1 and z_2 by finding the value which best predicts the mean optical depth, defined by $\bar{\tau}_\alpha \equiv -\log\langle\exp(-\tau)\rangle$ averaged over the spectra, at $z = z_2$ using the spectra at $z = z_1$. (In principle, a different value for α may be found by reversing the roles of z_1 and z_2. We checked this and found in all cases the same value for α was derived.) The values found are provided in Tables 3 and 4. We allow for an overall rescaling of the radiation field by multiplying the optical depths by a scale factor s. (The factor s could also be interpreted as a rescaling of the baryon density, although this would entail a change in the gas temperature, which we do not allow for.) The UV background radiation field adopted in the simulations evolves according to the model of Haardt & Madau (1996) predicted for QSOs as the sources of the radiation, and assuming an intrinsic QSO spectral index $\alpha_Q = 1.5$. The radiation field is turned on at $6 < z_{\rm ion} < 7$. We additionally accommodate an alternative evolution in the radiation field by allowing for a further evolution factor $(1+z)^p$ multiplying the Haardt & Madau rate $\Gamma_{\rm HM}(z)$. Thus we predict τ at any given wavelength λ at redshift z based on the value at redshift z_1 at wavelength $\lambda(1+z)/(1+z_1)$ according to

$$\tau(z) = s\tau(z_1)\left(\frac{1+z}{1+z_1}\right)^\alpha\left(\frac{1+z_{\rm ref}}{1+z}\right)^p\frac{\Gamma_{\rm HM}(z_1)H(z_1)}{\Gamma_{\rm HM}(z)H(z)}, \quad (1)$$

where $z_{\rm ref}$ is a reference redshift introduced for $p \neq 0$. The values for s, p, and $z_{\rm ref}$ adopted for different cosmologies and required to match the measured spectra are provided below.

The interpolation to intermediate redshifts to cover the wavelength range of a particular measured spectrum is performed by generating spectral segments from the simulations, each a fixed redshift interval $\Delta z = 0.1$ in length, scaling the optical depth in each segment according to equation 1, and then effectively piecing the segments together to match the wavelength range of the measured spectrum. In order to interpolate between two data dumps at redshifts z_1 and z_2, we compute the distribution functions $f(x; z, z_d)$ for any given statistic x within a redshift interval $(z, z+\Delta z)$ by first extrapolating the optical depths from a data dump at z_d to z, and then computing the final distribution function for a redshift interval $z_b < z < z_a$ according to

$$f(x) = \sum_i \Delta z\left[w_{2,i}f(x; z_i, z_1) + w_{1,i}f(x; z_i, z_2)\right], \quad (2)$$

using the linear weights $w_{j,i} = |(z_i - z_j)/(z_2 - z_1)|$, and incrementing z_i from z_b to z_a. We find this procedure recovers the distribution functions at intermediate redshifts to very high accuracy, as is shown in Appendix A.

In all cases, the wavelength coverage $z_b < z < z_a$ corresponds to a range between Lyα and Lyβ in the QSO restframe to avoid confusing Lyβ absorption with Lyα absorption. In practice the ranges are usually shortened to a smaller interval, depending on the wavelength coverage of the spectrum and to avoid the local photoionizing influence of the QSO (the proximity effect).

A major uncertainty in comparing with the measured spectra is the setting of the continuum level. Normally peak flux points are used to determine the level of the continuum in the Lyα forest region of the spectrum. In regions where the flux never recovers to the true continuum, however, this procedure will result in an underestimate of the true continuum level. Without an automated procedure for inferring the continuum within the forest, it is difficult to gauge the effect of the uncertainty in the continuum level. We find that making no correction to the continuum frequently results in a mismatch in the flux distribution for flux values near unity (in units of the continuum). We model errors in the continuum level by allowing for a shift in its overall value according to:

$$F_i = \frac{F_i^{(0)}}{1-\omega}, \quad (3)$$

where $F_i^{(0)}$ is the flux predicted by the numerical model at pixel i, and F_i is a corrected flux allowing for a downward shift in the continuum level by the fractional amount ω, applied uniformly across the spectrum. This is a crude approximation to the actual errors likely to occur. We adopt it for its simplicity in order to assess the impact of possible continuum errors. For a more accurate comparison, it would be necessary to re-analyse the raw data and offset the simu-

lation spectra at each pixel following a procedure consistent with that of the observers.

The fitting of absorption lines to the spectra requires a noise value for each pixel. We generate a noise matrix from the 1σ noise levels in the observed spectra, averaging the noise in several flux bins over redshift intervals of width $\Delta z = 0.1$. We then draw a noise value assuming the noise to be gaussian distributed with a standard deviation corresponding to the matrix element of the redshift and flux of the pixel. This allows us to model a varying signal–to–noise ratio across a spectrum, and allows for a correlation between flux and noise. We have verified that the statistical properties of the spectra are not very sensitive to the noise model: averaging over redshift bins but not allowing for a correlation between flux and noise level yields very similar results.

2.2 Statistical analysis tools

There are several statistics that may be used as a basis of comparison between the models of the Lyα forest and the observed spectra. The most fundamental is simply the distribution of flux per pixel. A high level of degree of accuracy in the cumulative flux distribution may be achieved because of the large number of pixels in the spectra. The measured and predicted cumulative distributions may be compared using the Kolmogorov–Smirnov (KS) test, for which the expected value of the difference (in absolute value) $d_{\rm KS}$ between the distributions for N measurements is $\bar{d}_{\rm KS} \simeq 0.9/N^{1/2}$, and $d_{\rm KS}$ should exceed $1.6/N^{1/2}$ only 1 per cent of the time. For a typical number of pixels $N \sim 10^4$, the agreement between the predicted and measured cumulative flux distributions should then be $d_{\rm KS} \approx 0.01$. The probability distribution is based on the assumption that the measurements are statistically independent. Because the absorption features will introduce correlations between neighbouring pixel fluxes (as will the resolution of the spectrographs), this assumption is formally violated. As is shown in Appendix A, the correlations effectively tend to reduce the number of independent pixels by a factor of 3–5. Even allowing for this, the test still provides a powerful means of quantifying the statistical agreement between the model predictions and the measured spectra.

Additional constraints are provided by the fluctuations in the spectra, which are related both to the underlying baryon density fluctuations and to the thermal and velocity widths of the associated absorption lines. We quantify the fluctuations in two ways. The scales of fluctuation of the spectral features may be directly characterised using the Discrete Wavelet Transform, which quantifies the changes in a given spectrum on being smoothed from one velocity resolution scale to another (Meiksin 2000). A multiscale analysis based on the Daubechies wavelets effectively performs a smoothing of the spectrum over successive doublings of the pixel width, weighted such that the spectrum is decomposed into orthogonal components corresponding to different velocity scales. (We use the Daubechies wavelet of order 20.) A wavelet analysis offers several advantages over the more traditional Voigt-profile absorption line analysis: 1. the method is objective, in that it does not require making arbitrary decisions regarding the deblending of absorption lines or the acceptability of a fit; 2. the method produces a large number of wavelet coefficients, $N/2^L$ at the resolution level L for N total pixels, corresponding to a typical $d_{\rm KS} \approx 0.01 \times 2^{L/2}$, thus enabling stringent statistical constraints to be set; 3. the coefficient distributions are insensitive to noise (Meiksin 2000); 4. the analysis is extremely fast. Monte Carlo simulations show that the wavelet coefficients are only weakly correlated, so that they may be treated as statistically independent (Meiksin 2000). There are, however, some disadvantages as well: 1. the light fluctuations are quantified only over successive doublings of the pixel size, allowing only coarse velocity resolution in the statistical quantification of the fluctuations; 2. the method is indifferent to the origin of the fluctuations, and in particular does not distinguish directly between the effects of H I column density and Doppler broadening, which may especially become mixed in the presence of substantial line-blending. For these reasons, we perform Voigt profile analyses as well.

We utilise AutoVP (Davé et al. 1997) to decompose the spectra into a set of Voigt absorption line profiles. Typically 300–500 lines are found per spectrum, providing a precision of $d_{\rm KS} \approx 0.05$ in the cumulative distributions of $N_{\rm HI}$ and b. In order to determine the sensitivity of the resulting distributions of absorption line parameters to the line analysis method, we have also developed a separate algorithm called SPECFIT. Rather than searching for absorption maxima, and adjusting the number of lines required for a good fit, as does AutoVP, SPECFIT first splits the spectra into segments bordered by flux values above that corresponding to a minimum optical depth threshold $\tau_{\rm min}$, and then searches for inflection points in noise-filtered representations of the data in each segment in order to identify the locations of candidate absorption lines. The candidate lines are then fit to the original spectrum. While less sophisticated than AutoVP, SPECFIT operates a factor of 50-100 faster with a comparable level of success in the fits, except that it sometimes misses the weakest optically thin features ($\tau < \tau_{\rm min}$). The two methods are compared in Appendix B.

In the following, we shall generally regard the 3σ level (a KS test probability of $P_{\rm KS} = 0.001$) as the threshold for rejecting a predicted distribution compared with the measured using the KS test.

2.3 Data

We compare the simulation results with six Keck HIRES spectra and one VLT UVES spectrum that have been published in the literature. The quasars, the redshift range used in the comparison, the pixel resolutions of the spectra, and the spectral resolutions, are summarised in Table 2. All the spectra were normalized to a unit continuum level by the observers.

3 RESULTS

In this section, we present comparisons between the simulations and the data as quantified by the flux per pixel distributions and the distributions of wavelet coefficients and absorption line parameters. Because of differences in the characteristics of the spectra and the dispersion in the statistics extracted from the measured spectra, we present the results

for each spectrum separately. The reader interested primarily in the implications of the results may choose to skip this section and proceed to Section 4.

The amplitudes of the distributions found in the models cannot be used as a basis of comparison since the optical depths may be arbitrarily rescaled for any individual model by the ionization bias factor $b_{\rm ion} \propto \Omega_b^{1.6}/\Gamma$ (Hui & Gnedin 1997; Croft et al. 1997). (We note the temperature–density relation found by Zhang et al. 1998 for systems in the column density range $12.5 < \log_{10} N_{\rm HI} < 14.5$ is consistent with this dependence.) The dependence on Ω_b is based on an approximate polytropic relation between density and temperature found to hold at low density (Meiksin 1994; Hui & Gnedin 1997), corresponding to the low and moderate column density systems which dominate the absorption in the spectra. The relationship, however, is not valid for higher column density systems ($\log_{10} N_{\rm HI} > 15$) because these arise predominantly in high density regions (Zhang et al. 1998), for which the relationship inverts (Meiksin 1994; Theuns et al. 1998b). The scaling also neglects the effects of changes in the gas temperature on absorption profiles that will result from a change in the baryon density, or of any associated pressure changes. For these reasons, it is most conservative to view a change in $b_{\rm ion}$ as a change in Γ, which has little effect on the gas temperature or pressure. It is important to normalize all the models consistently with any given measured QSO spectrum before comparing the shapes of any of the distributions with those measured. This may be accomplished in a variety of ways. We do so by matching the mean H I optical depth $\bar\tau_\alpha$ in each simulation to the measured intergalactic H I optical depth over the comparison redshift interval. Since the resulting model flux distributions will often mismatch the observed distributions for flux values near unity, we will also allow for a constant offset in the continuum as given by equation 3, while keeping the value of $\bar\tau_\alpha$ fixed at the observed value. In some instances it is also found necessary to introduce additional evolution in the UV radiation background to that adopted in the simulations.

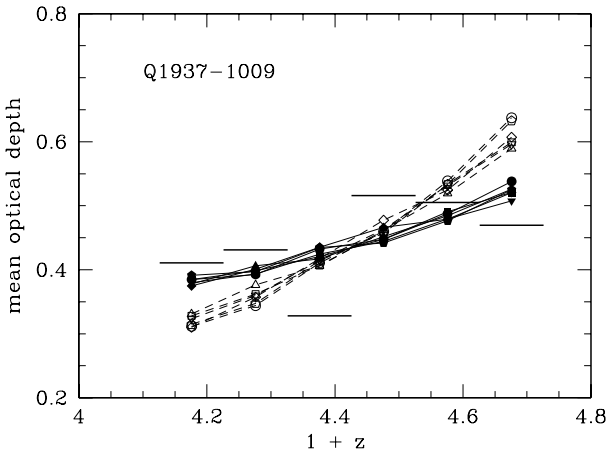

Figure 1. Redshift dependence of mean optical depth $\bar\tau_\alpha$ for Q1937−1009 (horizontal bars). The open symbols show the values for $\bar\tau_\alpha$ found in the simulations based on the evolution of the UV radiation background as determined from QSO sources by Haardt & Madau (1996). The filled symbols show the values for $\bar\tau_\alpha$ after allowing for an alternative redshift dependence of the UV radiation background. The symbols are: CHDM (circles), $\Lambda{\rm CDM_L}$ (squares), $\Lambda{\rm CDM_H}$ (diamonds), OCDM (triangles), SCDM (inverted triangles), tCDM (pentagons).

3.1 Q1937−1009

3.1.1 Flux distribution

We investigate Q1937−1009 (Burles & Tytler 1997) most thoroughly in order to assess the magnitude of some of the possible systematics in our analyses. Over the redshift range $3.126 < z < 3.726$, the mean optical depth in the measured spectrum is $\bar\tau_\alpha = 0.44$. The mean optical depths in redshift intervals $\Delta z = 0.1$ wide are shown in Fig. 1, along with estimates from each of the models. The optical depth per pixel has been rescaled according to equation 1 for each model, using the parameter values given in Table 3. We note that the redshift dependences for the optical depth per pixel found in the simulations are generally steeper than the dependence expected in a homogeneously expanding universe: $\tau(z) \propto (1+z)^6/H(z)$ (assuming constant Γ). By contrast, the measured values of the mean optical depth $\bar\tau_\alpha$ are nearly flat with redshift. Formally they are well fit by $\bar\tau_\alpha = a(1+z)^b$, with $a = 0.022^{+0.044}_{-0.015}$ and $b = 2.0 \pm 0.74$, where the standard deviation of the measured values of $\bar\tau_\alpha$ is adopted as a measurement error for each value. The models predict a near doubling of the mean optical depth over the same redshift interval, corresponding to $b = 6$, significantly steeper than measured. It is evident that an alternative evolution rate to that of the simulations is required to match the redshift dependence of the mean optical depths. To match the observed evolution, we adopt the additional rate exponents p for $z_{\rm ref} = 3$ (cf equation 1) as given in Table 3. The resulting distributions of $\bar\tau_\alpha$ for the various models are shown in Fig. 1.

The distributions of flux per pixel for the various models are compared with the observed distribution in Fig. 2. (Flux values exceeding unity result from noise fluctuations.) The agreement is generally good, particularly for the $\Lambda{\rm CDM_L}$ model. The models, however, all show some disagreement at flux values near unity, and for this reason they are all formally rejected by the KS test. For the $\Lambda{\rm CDM_L}$ model, the maximum difference (in absolute value) between the predicted and measured cumulative distributions is $d_{\rm KS} = 0.022$, corresponding to a formal acceptance probability of $P_{\rm KS} = 10^{-4}$. The next best model is SCDM, which gives $d_{\rm KS} = 0.039$ and $P_{\rm KS} = 8 \times 10^{-14}$.

Allowing for the possibility that the continuum level in the observed spectrum was set slightly low, resulting in overestimates of the normalized flux, we increase the flux per pixel according to equation 3, choosing values for s and ω that simultaneously preserve $\bar\tau_\alpha = 0.44$ and match the measured flux distribution at flux values near unity. The resulting flux distributions are shown in Fig. 3, using the values for s and ω in Table 3. The agreement in the cumulative dis-

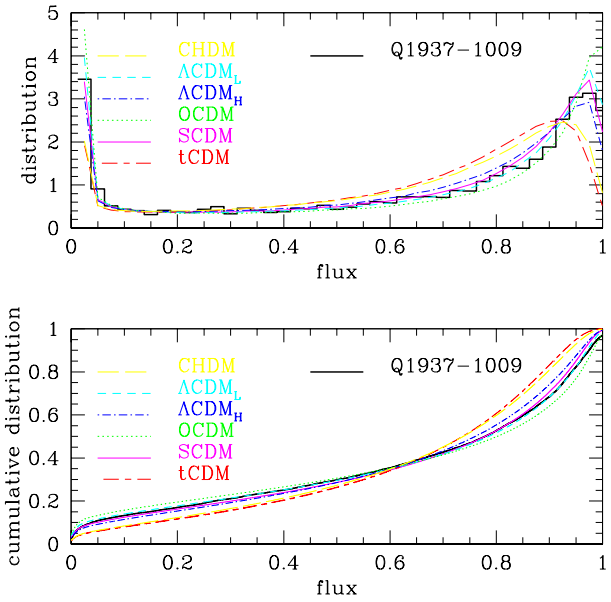

Figure 2. Comparison between the measured flux distribution of Q1937−1009 and the model predictions. Particularly good agreement is found for the $\Lambda\mathrm{CDM_L}$ model, although it is formally rejected by the KS test. (The measured distribution has been rebinned in the upper panel for clarity.)

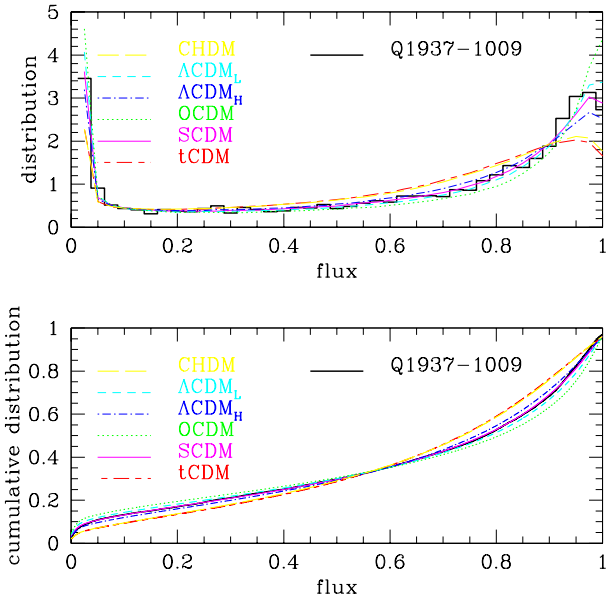

Figure 3. Comparison between the measured flux distribution of Q1937−1009 and the model predictions. A continuum offset is applied to each model to enforce matching the cumulative distributions at flux values near unity. The distributions tighten compared with Figure 2. The SCDM model is now preferred over $\Lambda\mathrm{CDM_L}$. (The measured distribution has been rebinned in the upper panel for clarity.)

tributions is now tightened, with the SCDM model agreeing best with the observed distribution. For the SCDM model, $d_{\mathrm{KS}} = 0.016$, corresponding to a formal acceptance probability by the KS test of $P_{\mathrm{KS}} = 0.011$. By comparison, the next best models are $\Lambda\mathrm{CDM_H}$ and $\Lambda\mathrm{CDM_L}$, with $d_{\mathrm{KS}} = 0.031$ and 0.033, respectively, both of which are strongly rejected by the KS test, with respective acceptance probabilities of $P_{\mathrm{KS}} = 4 \times 10^{-9}$ and 5×10^{-10}.

We recall that the KS test is based on the probability distribution of $N^{1/2} d_{\mathrm{KS}}$, where N is the number of independent measurements in the sample. In Appendix A, it is shown that the probability distribution for this quantity based on the simulated spectra is broader than the theoretical distribution, as may be expected if the flux values in neighbouring pixels are correlated. Because of the limited number of lines-of-sight drawn from the simulation volume, it is not possible to attach meaningful probabilities to large values of d_{KS} directly from the simulations. It is shown in Appendix A, however, that the probability distribution is close to that of the KS test for an effective number of pixels reduced by a factor of 3–5 from the actual number. Allowing for this reduction, the KS probabilities for the SCDM, $\Lambda\mathrm{CDM_H}$, and $\Lambda\mathrm{CDM_L}$ models (with continuum offsets applied) become, respectively, $P_{\mathrm{KS}} = 0.36 - 0.68$, 0.002–0.037, and 0.001–0.024, still favouring SCDM, but not excluding the ΛCDM models. The predictions of the CHDM, OCDM and tCDM models, however, are still strongly rejected. We note that not allowing for the continuum offset correction for $\Lambda\mathrm{CDM_L}$ gives the KS probability, allowing for the reduced effective number of pixels, $P_{\mathrm{KS}} = 0.081 - 0.29$, so that the $\Lambda\mathrm{CDM_L}$ model is perhaps no less viable than the SCDM model. The difference in the probability value with and without a continuum offset illustrates how susceptible P_{KS} is to even a small degree of uncertainty in the continuum level. We note that while each of the $\Lambda\mathrm{CDM_L}$ models disagrees with the measured flux distribution more than does the SCDM model, the predicted flux distributions bracket the measured distribution, so that an intermediate ΛCDM model may be expected to provide an even better match.

3.1.2 Wavelet coefficient distributions

The distribution of wavelet coefficients is shown in Fig. 4, both with no continuum offset applied and with the offsets in Table 3. The models generally show poor agreement with the measured distribution at the smallest velocity scale, $\sim 4 - 8\,\mathrm{km\,s^{-1}}$. It is possible that this is due to an inadequancy in the modelling of the spectral characteristics of the Keck HIRES in the synthetic spectra. Better agreement with Keck data, however, was achieved by Meiksin (2000) using similar modelling for a set of Monte Carlo realisations. It may be that the disagreement results from limitations of the simulations. We discuss this further in Section 4 below. A discrepancy is also found on the next scale of 8–17 $\mathrm{km\,s^{-1}}$, with half the models ($\Lambda\mathrm{CDM_L}$, OCDM and SCDM) exhibiting too great an amount of velocity structure (as indicated by the larger values of the coefficients). The discrepancy between these models and the data suggests a greater number of absorption features predicted by the simulations on these scales than in the data. The lower normalization models, by contrast, predict a smaller amount of structure than in the data, while the $\Lambda\mathrm{CDM_H}$ model is intermediate and agrees

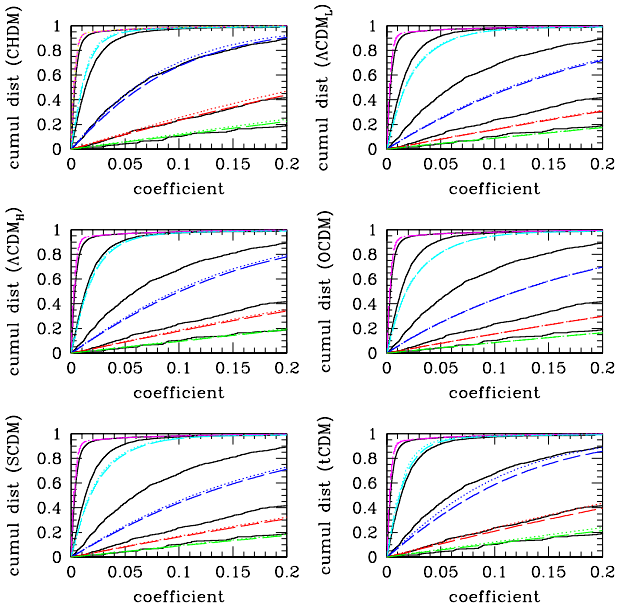

Figure 4. Comparison between the measured wavelet coefficient cumulative distributions of Q1937−1009 (solid curves) and the model predictions with (dashed curves) and without (dotted curves) continuum offset corrections. The curves from left to right correspond to the approximate velocity scales 4–8, 8–17, 17–34, 34–68, and 68–136 km s^{-1}. The predictions of the CHDM model agree best with the measured distributions.

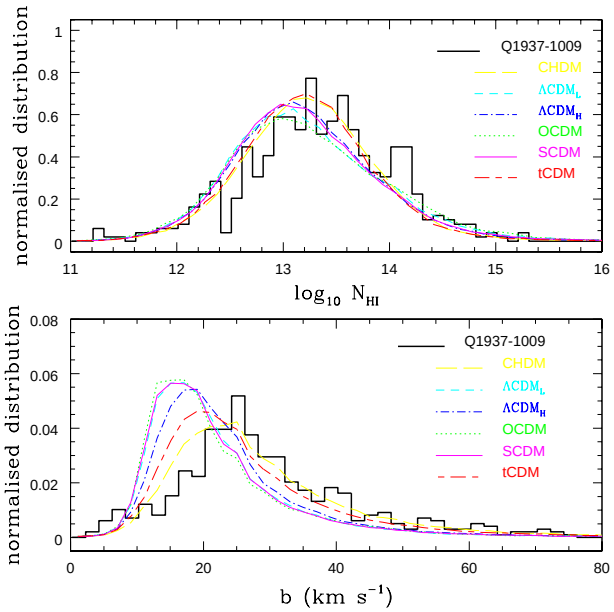

Figure 5. Comparison between the measured absorption line parameter distributions of Q1937−1009 and the model predictions using AutoVP, allowing for an offset in the continuum level. While good agreement is generally found for the $N_{\rm HI}$ distributions, the predicted b distributions are generally skewed toward lower b-values than measured. (The measured distributions have been rebinned for clarity of presentation.)

best with the data (though it is formally rejected by the KS test, with $d_{\rm KS} = 0.05$ and $P_{\rm KS} = 6 \times 10^{-7}$). The disagreement at the next velocity scale of 17–34 km s^{-1} is generally much worse. These velocities correspond to the typical Doppler parameters of the absorption features (see below). Only the CHDM model provides an acceptable match to the data on these scales; the other models predict far too much structure. The effect of the continuum offset correction is generally negligible on all velocity scales, except for CHDM and tCDM (which have the largest corrections), although it is small even for these. For CHDM, the KS test gives on the scale 17–34 km s^{-1}, $d_{\rm KS} = 0.041$ and $P_{\rm KS} = 0.030$ without the offset correction, and $d_{\rm KS} = 0.035$ and $P_{\rm KS} = 0.083$ with the correction. The agreement between the models and the data tends to improve for all the models at larger velocity scales.

3.1.3 Absorption line parameter distributions

The H I column density and Doppler parameter distributions resulting from fitting absorption lines to the spectra using AutoVP are shown in Fig. 5. The continuum offsets of Table 3 have been applied. For each model, effectively 50 separate spectra were constructed from the simulation box corresponding to the identical spectral range analysed in Q1937−1009. The profile analysis is computationally expensive. For the range of column densities of interest, it is adequate to fit the spectra using Doppler profiles rather than full Voigt profiles. We find there is little difference in the resulting distributions, while a factor of 2 is saved in the computing time. Typically $2-3\times10^4$ features in total are found for each model, requiring an analysis time of $\sim 1-2\times10^5$ cpu seconds on a Compaq XP900 with a 1GHz processor.

The agreement in the distribution of $N_{\rm HI}$ between the data and all the models is reasonably good, with the prediction of CHDM providing the best match, as is found in the wavelet analysis. The predicted b distributions for the remaining models peak at substantially lower values than does the measured distribution. For both the $N_{\rm HI}$ and b distributions, we find that the probability distribution for $N^{1/2}d_{\rm KS}$, where N is the number of absorption lines, is narrower than the theoretical distribution, so that the rejection probabilities provided by the KS test below are perhaps conservative. We discuss this point further in Appendix A.

The cumulative distributions are shown in Fig. 6. The measured $N_{\rm HI}$ distribution is best matched by the CHDM model: the maximum difference in the measured and predicted cumulative distributions is $d_{\rm KS} = 0.083$, with the associated formal KS acceptance probability $P_{\rm KS} = 0.002$. The next best model is tCDM, with $d_{\rm KS} = 0.10$ and $P_{\rm KS} = 4\times10^{-5}$. The CHDM model also provides the best match to the measured b distribution, with $d_{\rm KS} = 0.071$ and $P_{\rm KS} = 0.013$. (The remaining models are very strongly rejected; the next best is tCDM with $d_{\rm KS} = 0.16$ and $P_{\rm KS} = 4\times10^{-12}$.) It is clear that all the models other than CHDM predict far too narrow lines. The ΛCDM$_{\rm H}$ model, which yields the largest b-values of those models for which the predicted pixel flux distribution is consistent with the measured, predicts a median Doppler parameter of $b_{\rm med} = 20.9$ km s^{-1}. The mea-

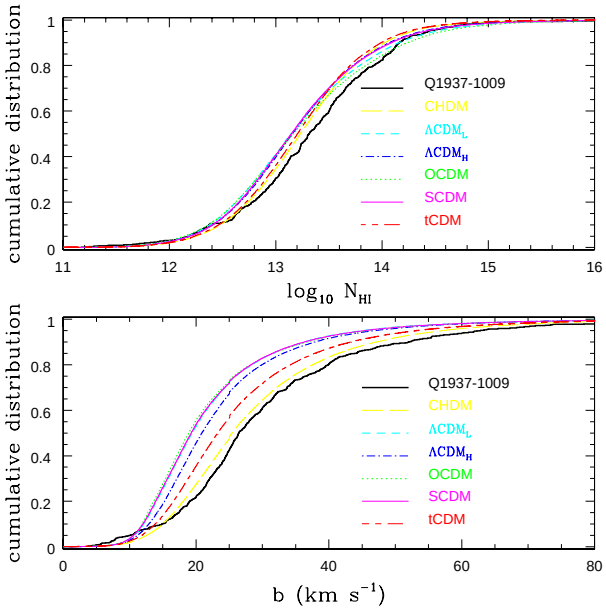

Figure 6. Comparison between the measured absorption line parameter cumulative distributions of Q1937−1009 and the model predictions using AutoVP, allowing for an offset in the continuum level. The predicted $N_{\rm HI}$ distributions tighten about the measured distribution. The CHDM model agrees best with the measured $N_{\rm HI}$ and b distributions.

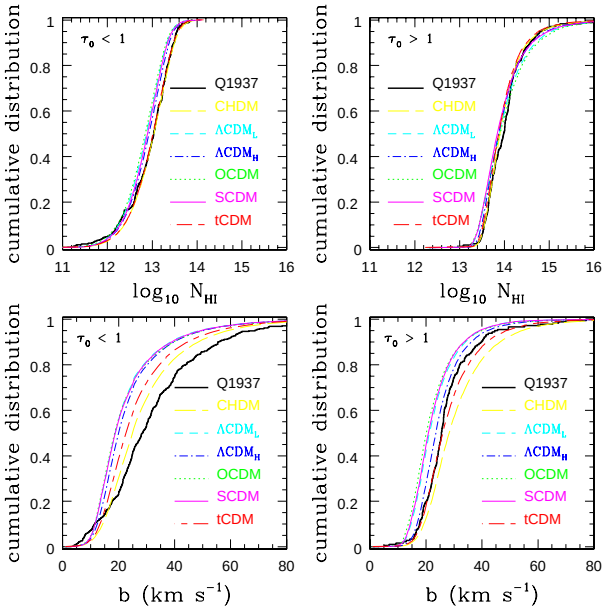

Figure 7. Comparison between the measured absorption line parameter cumulative distributions of Q1937−1009 and the model predictions using AutoVP, for subsamples of lines optically thin ($\tau_0 < 1$) and optically thick ($\tau_0 > 1$) at Lyα line-centre. The agreement between the model predictions and the data is best for the optically thick systems. All the models predict much too low median b-values for the optically thin systems.

sured median b is $26.4 \pm 0.9\,{\rm km\,s^{-1}}$ ⋆, too large by 6σ, but consistent with $b_{\rm med} = 25.5\,{\rm km\,s^{-1}}$ predicted by the CHDM model.

The narrowness of the absorption lines is reflected by the larger number of systems found in the AutoVP analyses of the simulation results: more lines are required to recover the mean measured optical depth of the spectrum. The AutoVP analysis of the spectrum of Q1937−1009 yields a total of 495 absorption features. The expected numbers of lines predicted by the models are for CHDM: 543; $\Lambda{\rm CDM_L}$: 592; $\Lambda{\rm CDM_H}$: 597; OCDM: 571; SCDM: 618, and tCDM: 585, all of which except CHDM exceed the measured number by at least 3σ, assuming Poisson fluctuations.

The effect of the continuum offset is small in comparison with the variances between the predicted and measured $N_{\rm HI}$ and b distributions. For instance, for the $\Lambda{\rm CDM_L}$ model, which provides the best fit to the pixel flux distribution without a continuum offset correction, the median Doppler parameter is $20.2\,{\rm km\,s^{-1}}$ with no offset correction and $19.4\,{\rm km\,s^{-1}}$ with the correction. Both values are inconsistent with the measured median b-value by over 6σ. The KS test formally strongly rejects the $N_{\rm HI}$ and b distributions, compared with the measured distributions, for both cases.

Absorption features with a line-centre optical depth $\tau_0 < 1$ correspond to structures that are underdense at $z = 3$, while higher optical depth systems are associated with overdense gas (Zhang et al. 1998). Underdense gas at these redshifts is too rarefied to maintain thermal equilibrium between photoionization heating and radiative losses, and so will retain a partial memory of its thermal history (Meiksin 1994). Overdense gas is more readily able to maintain thermal equilibrium. Because of this physical difference, we split the line samples into two subsamples at $\tau_0 = 1$ to determine if the disagreements between the measured and predicted $N_{\rm HI}$ and b distributions may be due to an incorrect thermal history rather than an incorrect cosmological model. The effect of this split is shown in Fig. 7. All of the models produce $N_{\rm HI}$ distributions for $\tau_0 > 1$ consistent with the data. The best case is CHDM, with $d_{\rm KS} = 0.10$ and $P_{\rm KS} = 0.041$. The worst cases are the SCDM and tCDM models, both with $d_{\rm KS} = 0.14$ and $P_{\rm KS} = 0.002$, while the $\Lambda{\rm CDM_L}$ and $\Lambda{\rm CDM_H}$ models give, respectively, $d_{\rm KS} = 0.12$, $P_{\rm KS} = 0.014$ and $d_{\rm KS} = 0.11$, $P_{\rm KS} = 0.018$. Only the tCDM model is able to reproduce the b distribution for $\tau_0 > 1$ ($d_{\rm KS} = 0.06$, $P_{\rm KS} = 0.50$). All the models predict a number of absorption systems consistent with the measured number of 179 (CHDM: 149; $\Lambda{\rm CDM_L}$: 205; $\Lambda{\rm CDM_H}$: 184; OCDM: 214; SCDM: 206; tCDM: 161).

The disagreement between the model predictions and measured distributions for the $\tau_0 < 1$ systems is more se-

⋆ The error in the median is $(0.5\pi/N)^{1/2}\sigma$, where σ is the standard deviation of the distribution of b-values, N is the number of lines, and assuming the distribution of b-values is a guassian. The data and the simulations show a long tail toward high values, and so the error estimate should be modified accordingly (Kendall & Stuart 1969). We find that a lognormal distribution provides an acceptable fit to the distribution of b-values derived by AutoVP. Using the lognormal distribution instead of a gaussian changes the error on the median by less than one per cent.

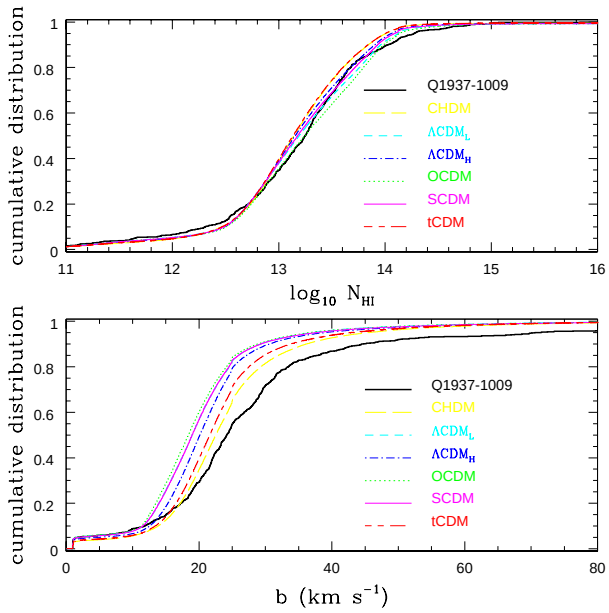

Figure 8. Comparison between the measured absorption line parameter cumulative distributions of Q1937−1009 and the model predictions using SPECFIT, allowing for an offset in the continuum level.

vere. None of the models is able to reproduce the measured b distribution. While the CHDM and tCDM models predict the correct shape for the $N_{\rm HI}$ distribution (both models give $d_{\rm KS} = 0.06$ and $P_{\rm KS} = 0.2$), they predict far too great a number of optically thin ($\tau_0 < 1$) lines compared with the measured number of 316, as do all the models except OCDM (CHDM: 395; ΛCDM$_{\rm L}$: 388; ΛCDM$_{\rm H}$: 413; OCDM: 357; SCDM: 414; tCDM: 426). Thus it appears the discrepancy between the model predictions and measured distributions arises primarily from the optically thin systems, although there is still a pronounced tendency for the models that agree best with the pixel flux distribution to predict too low b-values even for the optically thick ($\tau_0 > 1$) absorbers.

We note that the measured median Doppler parameter for the optically thin systems, $b_{\rm med} = 28.6 \pm 1.3\,{\rm km\,s^{-1}}$, is significantly higher than for the optically thick systems, $b_{\rm med} = 25.6 \pm 1.0\,{\rm km\,s^{-1}}$. This is opposite the trend of a decreasing envelope of b-values for optically thin systems found at lower redshift (Hu et al. 1995; Kirkman & Tytler 1997). It is also opposite the trend found in the simulations. The model predictions for $b_{\rm med}$ among the optically thick systems are for CHDM: $27.7\,{\rm km\,s^{-1}}$; ΛCDM$_{\rm L}$: $20.9\,{\rm km\,s^{-1}}$; ΛCDM$_{\rm H}$: $23.1\,{\rm km\,s^{-1}}$; OCDM: $18.8\,{\rm km\,s^{-1}}$; SCDM: $20.4\,{\rm km\,s^{-1}}$; tCDM: $25.3\,{\rm km\,s^{-1}}$. Of these, only the CHDM, ΛCDM$_{\rm H}$, and tCDM models are consistent with the measured value. The predictions for $b_{\rm med}$ for the optically thin systems, however, are substantially smaller: CHDM: $24.6\,{\rm km\,s^{-1}}$; ΛCDM$_{\rm L}$: $18.4\,{\rm km\,s^{-1}}$; ΛCDM$_{\rm H}$: $19.6\,{\rm km\,s^{-1}}$; OCDM: $18.2\,{\rm km\,s^{-1}}$; SCDM: $18.5\,{\rm km\,s^{-1}}$; tCDM: $22.1\,{\rm km\,s^{-1}}$. Only the CHDM model is able to match the high measured value within 3σ. We return to a discussion of this discrepancy in § 4.4 below.

To test the sensitivity of the distributions of absorption line parameters to the line-analysis method, we perform a second set of analyses using SPECFIT. The results are shown in Fig. 8. The adopted threshold optical depth for finding lines is $\tau_{\rm min} = 0.15$, although smaller optical depth lines may result from the fits. (It would have been possible to use a smaller value for $\tau_{\rm min}$ for most of the models; the value adopted was required by the CHDM and tCDM models to avoid producing an excessive number of lines. The same value was adopted for the analysis of all the models for consistency.) The best fits to the measured $N_{\rm HI}$ distribution are provided by the ΛCDM$_{\rm L}$ and SCDM models, allowing for continuum offset corrections. The predicted CHDM and tCDM $N_{\rm HI}$ distributions do most poorly, both being significantly steeper than the measured distribution. The KS test applied to the ΛCDM$_{\rm L}$ and SCDM results gives, respectively, $d_{\rm KS} = 0.046$, $P_{\rm KS} = 0.16$ and $d_{\rm KS} = 0.056$, $P_{\rm KS} = 0.043$. The remaining models do significantly more poorly, giving for CHDM: $d_{\rm KS} = 0.086$, $P_{\rm KS} = 2 \times 10^{-4}$; ΛCDM$_{\rm H}$: $d_{\rm KS} = 0.073$, $P_{\rm KS} = 0.003$; OCDM: $d_{\rm KS} = 0.073$, $P_{\rm KS} = 0.003$; tCDM: $d_{\rm KS} = 0.092$, $P_{\rm KS} = 6 \times 10^{-5}$. In contrast to the AutoVP analysis, for which the CHDM model provides a marginally acceptable fit, the $N_{\rm HI}$ distribution derived for CHDM using SPECFIT provides a poor match to the data. By contrast, while the SPECFIT distributions for the ΛCDM$_{\rm L}$ and SCDM models are acceptable, the AutoVP distributions for these models are strongly rejected.

As was found in the AutoVP analysis, the models predict too low b-values: none of the models produces a b distribution consistent with the measured distribution. The measured median b-value is $24.2 \pm 1.8\,{\rm km\,s^{-1}}$, where the large error is due to the wide dispersion in b-values. All the model predictions are smaller, but only that of OCDM by more than 3σ. The SPECFIT analysis generally shows good consistency in the predicted number of absorption features. The analysis of the spectrum of Q1937−1009 yields 609 absorption features. The expected numbers of lines predicted by the models are for CHDM: 658; ΛCDM$_{\rm L}$: 527; ΛCDM$_{\rm H}$: 596; OCDM: 462; SCDM: 557, and tCDM: 661. Allowing for Poisson fluctuations, all the model predictions are consistent with the measured number except for ΛCDM$_{\rm L}$ and OCDM, which are too low. Thus, although the ΛCDM$_{\rm L}$ model predicts the correct shape for the $N_{\rm HI}$ distribution, it predicts an incorrect normalization.

The differences in the AutoVP and SPECFIT results may be due in part to the different relative emphasis the algorithms give to optically thin and optically thick systems. Splitting the SPECFIT results at $\tau_0 = 1$ shows that while all the models predict a number of lines with $\tau_0 > 1$ consistent (at the 3σ level) with the measured number of 178 (CHDM: 165; ΛCDM$_{\rm L}$: 192; ΛCDM$_{\rm H}$: 185; OCDM: 189; SCDM: 194, and tCDM: 170), only the CHDM, ΛCDM$_{\rm H}$ and tCDM models predict a number of optically thin lines consistent with the measured number of 431. (These models predict 493, 412 and 491 lines, respectively.) The OCDM and ΛCDM$_{\rm L}$ predictions lie over 3σ too low, while the CHDM and tCDM predictions are marginally consistent with the 3σ upper limit. This contrasts with the AutoVP results, for which all the models predicted too many optically thin systems. The two algorithms also yield differing levels of acceptability of the shapes of the $N_{\rm HI}$ distributions for the optically thin systems. While the AutoVP distributions agree well with the data for the CHDM and tCDM models, the SPECFIT results

are inconsistent with the data for all the models, except for the marginal case of tCDM ($d_{\rm KS} = 0.09$, $P_{\rm KS} = 0.001$).

The results of AutoVP and SPECFIT agree more closely for the optically thick systems, although still with some disagreement. While the AutoVP analysis yields acceptable $N_{\rm HI}$ distributions for all the models (although the results for the SCDM and tCDM models are marginal), the SPECFIT analysis yields distributions that are rejected for all the models except CHDM ($d_{\rm KS} = 0.08$, $P_{\rm KS} = 0.01$), although the $\Lambda{\rm CDM_L}$ and OCDM predictions are marginal (both give $d_{\rm KS} = 0.14$ and $P_{\rm KS} = 0.001$). Thus the acceptability of the predicted $N_{\rm HI}$ distributions is somewhat sensitive to the line-fitting algorithm used. This is due in part to the marginality of the rejection levels: a small change in the distributions pushes the level of agreement above or below the 3σ rejection threshold. Both algorithms nevertheless agree that the CHDM model provides the best match to the measured $N_{\rm HI}$ distribution for the optically thick systems.

No significant difference is found in the median measured b-values for the optically thin and thick systems using SPECFIT. For $\tau_0 < 1$, $b_{\rm med} = 24.5 \pm 2.3\,{\rm km\,s^{-1}}$; for $\tau_0 > 1$, $b_{\rm med} = 24.1 \pm 2.2\,{\rm km\,s^{-1}}$. Although all the models predict lower values for the median b-value than measured, for both $\tau_0 < 1$ and $\tau_0 > 1$ systems, the differences are not highly significant given the large errors in the measured values. A stronger statistical statement is made using the full sample. We note that the models predict that the optically thin systems will have smaller median Doppler parameters than the optically thick systems, but the differences are small, amounting to only 1–2 ${\rm km\,s^{-1}}$.

Just as is found for the full sample, the predicted b distributions for both the $\tau_0 < 1$ and $\tau_0 > 1$ subsamples are rejected by the KS test for all the models. The only exception is the marginal agreement found for the CHDM model for the optically thin systems ($d_{\rm KS} = 0.13$, $P_{\rm KS} = 0.004$). The SPECFIT analysis consistently finds that the models predict too low b-values compared with the data. This contrasts with the AutoVP analysis, for which the b distribution predicted by tCDM for optically thick systems provides an excellent match to the data (while all other model predictions are rejected).

It appears difficult to reach any definite conclusion regarding the goodness-of-fit of the predicted Doppler parameter distributions to the data. It is possible that AutoVP and SPECFIT cue off low optical depth fluctuations differently. The main lesson is likely that there is a limit to the physical interpretation of gas temperature or velocity dispersion that may be attached to the fit Doppler parameters.

3.2 HS 1946+7658

Recent CMB experiments strongly favour a flat, or nearly flat, universe (Netterfield et al. 2001; Pryke et al. 2001; Stompor et al. 2001). From hereon, we restrict the consideration of models to those currently most viable: CHDM, the two ΛCDM models, and tCDM. Although the tCDM model is perhaps already excluded by the CMB data, it provides useful comparisons with the predictions of the CHDM model and illustrates the degree to which simulations of the Lyα forest may (or may not) be used to discriminate between cosmological models based on the tests considered in this paper.

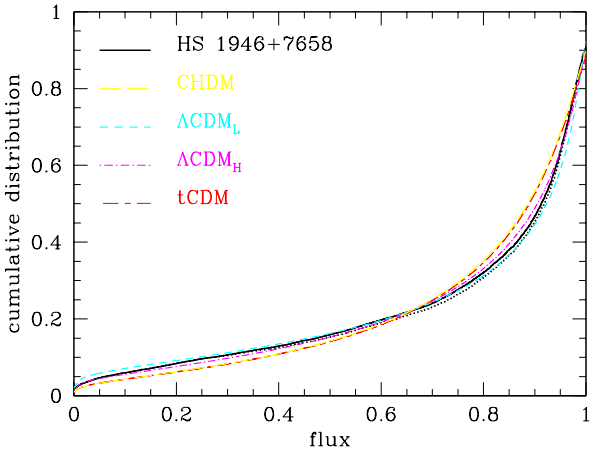

Figure 9. Comparison between the measured flux distribution of HS 1946+7658 and the model predictions. A continuum offset correction is applied to each model to enforce matching the cumulative distributions at flux values near unity. The dotted curve shows the measured cumulative flux distribution after removing pixels contaminated by identified metal lines. The best matches are obtained by the $\Lambda{\rm CDM_L}$ and $\Lambda{\rm CDM_H}$ models, with predicted distributions that bracket the measured one.

3.2.1 Flux distribution

Over the redshift range $2.5 < z < 3.0$, the mean optical depth in the spectrum of HS 1946+7658 is found to be $\bar{\tau}_\alpha = 0.24$. The adopted optical depth rescalings and conitnuum offset corrections for these models are provided in Table 4. No additional evolution in the UV background was required ($p = 0$).

The predicted and measured distributions of flux per pixel (excluding bad pixels and the region occupied by a Damped Lyα Absorber for the measured distribution), are shown in Fig. 9. Also shown is the measured flux per pixel distribution after removing pixels contaminated by metal lines identified by Kirkman & Tytler (1997). (We note that $\bar{\tau}_\alpha$ is negligibly affected by the removal of these regions.) The best matches to the measured metal-free distribution are provided by the $\Lambda{\rm CDM_L}$ and $\Lambda{\rm CDM_H}$ models, with the respective maximum cumulative distribution differences from that measured of $d_{\rm KS} = 0.047$ and $d_{\rm KS} = 0.039$. Both models are strongly ruled out by the formal KS test probability. Allowing for a reduction in the effective number of pixels by a factor 3–5 (Appendix A) still yields unacceptable probabilities for the predictions. The two model distributions, however, bracket the measured distribution, so it is reasonable to expect a ΛCDM model with an intermediate value of $\sigma_{\rm J}$ would provide an acceptable fit.

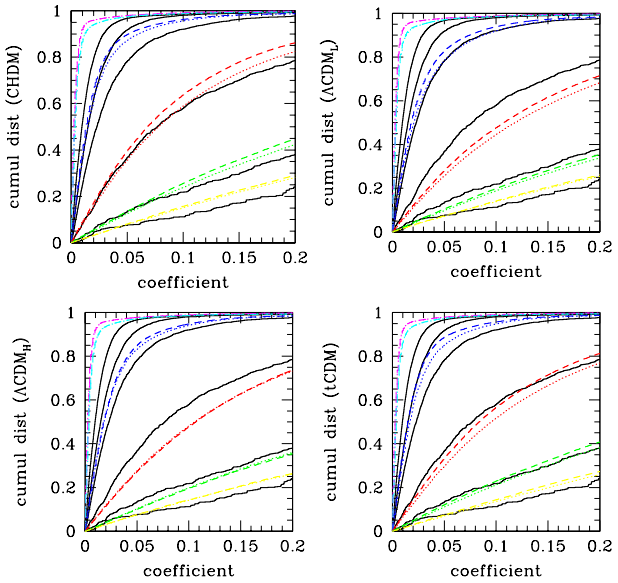

Figure 10. Comparison between the measured wavelet coefficient cumulative distributions of HS 1946+7658 (solid curves) and the model predictions extrapolating about the simulation data at $z = 3$ (dashed curves) and interpolating between the simulation data at $z = 2$ and $z = 3$ (dotted curves), allowing for continuum offset corrections in both. (For ΛCDM$_{\rm H}$, the dashed curves correspond to interpolation between the simulation data at $z = 2.7$ and $z = 3$.) The curves from left to right correspond to the velocity scales 2–4, 4–8, 8–16, 16–32, 32-64, and 64-128 km s^{-1} . The best match for the velocity scale 16–32 km s^{-1} , corresponding to the median measured Doppler parameter of the absorption features, is found for the CHDM and tCDM models. All the models underpredict the amount of velocity structure on smaller scales.

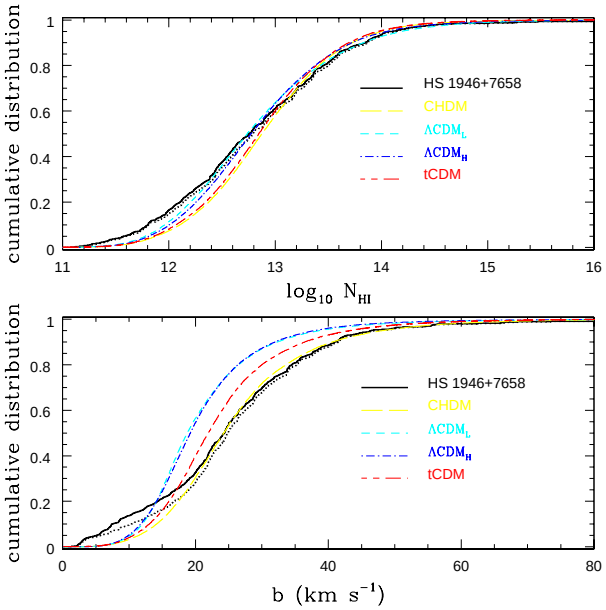

Figure 11. Comparison between the measured absorption line parameter distributions of HS 1946+7658 (solid curves) and the model predictions. While good agreement is generally found for the $N_{\rm HI}$ distributions above 10^{13} cm^{-2} , all the models underpredict the number of lower column density systems. The CHDM model best reproduces the measured b distribution. The agreements improve when metal absorption systems identified in the observed spectrum are removed (dotted curves).

3.2.2 Wavelet coefficient distributions

The wavelet coefficient distributions are shown in Fig. 10. All the models poorly match the velocity structure on scales of 8–16 km s^{-1} and smaller, indicating the presence of substantially more structure in the data on these scales than predicted by the models. This structure reflects at least in part the presence of metal lines.

Because the IGM temperature decreases with time in underdense regions, within which the more abundant optically thin features arise, it is unclear whether the best strategy for generating the distributions is by interpolating beteen the simulation results at $z = 2$ and $z = 3$ or by extrapolating the optical depths from the $z = 3$ results alone, as the spectral range analyzed lies nearer $z = 3$ than $z = 2$. The distributions for both approaches are shown in Fig. 10. The results of both methods are qualitatively similar. (We note that the two approaches produce negligible differences in the flux distributions.) Neither approach yields a good match at low velocity scales. On the scale 16–32 km s^{-1} , corresponding to the median measured Doppler parameter (see below), acceptable agreement is found for the CHDM results based only on interpolation ($d_{\rm KS} = 0.042$, $P_{\rm KS} = 0.026$), while agreement for tCDM is found only for extrapolating from $z = 3$ ($d_{\rm KS} = 0.045$, $P_{\rm KS} = 0.015$). The agreement tends to improve for all the models on larger velocity scales.

3.2.3 Absorption line parameter distributions

All the models underpredict the number of low H I column density systems and low b-value systems, as shown in Fig. 11. It is possible that the low $N_{\rm HI}$ and low b-value systems in the measured spectrum are dominated by metal absorption features. Kirkman & Tytler (1997) identify a large number of metal lines in the redshift range analysed. Unfortunately, because these lines are frequently blended with Lyα forest systems, it is not possible to match them on a one-to-one basis with the lines produced by AutoVP. In an attempt to account for the metal absorbers, we remove a narrow line ($b < 15$ km s^{-1}) from our list when it matches against a metal absorber in the list of Kirkman & Tytler (1997) to within a tolerance of 2Å in the (observed) line-centre wavelength. This results in the rejection of 28 systems. The resulting cumulative distributions, shown by the dotted curves in Fig. 11, match the predicted more closely. Formally, all the $N_{\rm HI}$ distributions are acceptable at the 3σ level by the KS test. The best matches are provided by the ΛCDM$_{\rm L}$ and ΛCDM$_{\rm H}$ models, which give for ΛCDM$_{\rm L}$: $d_{\rm KS} = 0.063$, $P_{\rm KS} = 0.057$; and for ΛCDM$_{\rm H}$: $d_{\rm KS} = 0.064$, $P_{\rm KS} = 0.053$. Similar results are obtained either by interpolating between the $z = 2$ and $z = 3$ simulation results, or extrapolating from the $z = 3$ results alone. Only the CHDM model yields a b distribution consistent with the data. The KS test gives

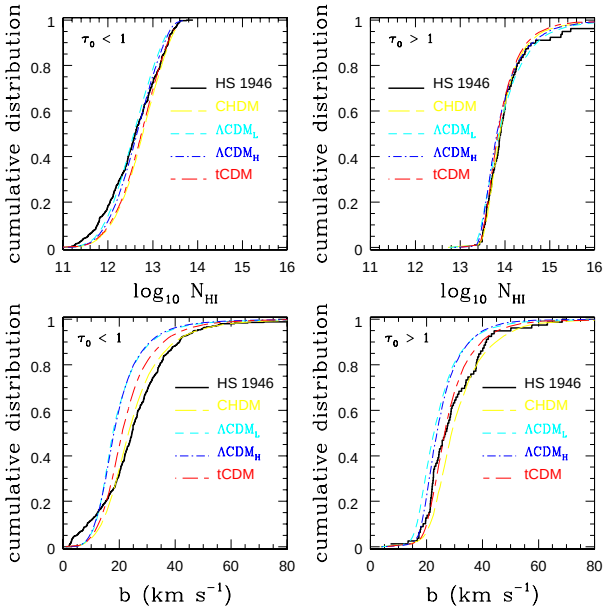

Figure 12. Comparison between the measured absorption line parameter distributions of HS 1946+7658 and the model predictions, for systems with $\tau_0 < 1$ and $\tau_0 > 1$. The predicted distributions agree better with the measured distributions for the optically thick systems than for the optically thin.

$d_{\rm KS} = 0.065$, $P_{\rm KS} = 0.048$, extrapolating from the $z = 3$ simulation results. An inconsistent distribution results when based on interpolation between the $z = 2$ and $z = 3$ results because of the lower b-values at $z = 2$.

As was the case for Q1937−1009, the models that provide the best fits the flux distribution (ΛCDM$_{\rm L}$ and ΛCDM$_{\rm H}$) predict too small median Doppler parameters. The measured median b (after excluding metal lines) is $24.9 \pm 0.8\,{\rm km\,s^{-1}}$, while ΛCDM$_{\rm L}$ and ΛCDM$_{\rm H}$ predict, respectively, $18.8\,{\rm km\,s^{-1}}$ and $19.2\,{\rm km\,s^{-1}}$, both too small by over 7σ.

The AutoVP analysis of the spectrum of HS 1946+7658 yields 443 absorption lines. The predicted numbers for the various models are for CHDM: 508; ΛCDM$_{\rm L}$: 539; ΛCDM$_{\rm H}$: 565; and tCDM: 539, all greatly in excess of the measured number except for CHDM. The larger predicted numbers are consistent with the general narrowness of the features.

As for Q1937+1009, we split the line samples into two subsamples, optically thin ($\tau_0 < 1$) and optically thick ($\tau_0 > 1$) at line-centre. The resulting $N_{\rm HI}$ and b distributions (with identified metal lines removed as above) are shown in Fig. 12. Excellent agreement is found between the model predictions for the $N_{\rm HI}$ distribution and the measured distribution for the optically thick systems. Acceptable agreement (at the 3σ level) is found for the b distributions as well, except for the ΛCDM$_{\rm L}$ model, which is marginally rejected by the KS test. The agreement for the optically thin systems is much poorer. Only the ΛCDM models yield acceptable $N_{\rm HI}$ distributions, while only the CHDM model predicts a b distribution consistent with the measured. The measured b distribution disagrees most strongly with the CHDM prediction at $b < 15\,{\rm km\,s^{-1}}$. Although we match 28 metal lines with the list of Kirkman & Tytler, they report 45 in the redshift range of interest, which could potentially account for the difference. We note that these CHDM results are based on extrapolating from the $z = 3$ simulation results; the distribution derived by interpolating between the $z = 2$ and $z = 3$ results yields unacceptably small b-values, as for the other models.

The AutoVP analysis of the spectrum of HS 1946+7658 yields 79 absorption systems with $\tau_0 > 1$ and 364 with $\tau_0 < 1$. The predicted numbers of optically thick features for the various models are for CHDM: 68; ΛCDM$_{\rm L}$: 102; ΛCDM$_{\rm H}$: 92; and tCDM: 76, all consistent with the measured number within Poisson fluctuations. The predicted numbers of optically thin features for the models are for CHDM: 440; ΛCDM$_{\rm L}$: 437; ΛCDM$_{\rm H}$: 473; and tCDM: 463. All the model predictions greatly exceed the number of measured lines.

3.3 Q0014+813, Q0302−003, Q0636+680, Q0956+122

3.3.1 Flux distribution

The analysis redshift ranges for each of the Hu et al. (1995) QSO spectra are given in Table 2. The mean optical depth found for each is: Q0014+813: $\bar{\tau}_\alpha = 0.30$; Q0302−003: $\bar{\tau}_\alpha = 0.31$; Q0636+680: $\bar{\tau}_\alpha = 0.29$; Q0956+122: $\bar{\tau}_\alpha = 0.25$. It was found unnecessary to include any amount of additional evolution in the UV radiation background. The adopted optical depth rescalings and continuum offsets are given in Table 5.

The distributions of flux per pixel are shown in Fig. 13. The best-fitting model is ΛCDM$_{\rm L}$ in all cases except Q0956+122, for which it is ΛCDM$_{\rm H}$. Formally, all the models are rejected by the KS test. Allowing for a reduction in the effective number of pixels by a factor of 3–5 due to correlations between neighbouring pixel values yields acceptable agreement. The maximum differences between the measured cumulative distributions and those predicted by the ΛCDM$_{\rm L}$ model, and the associated probabilities, are for Q0014+813: $d_{\rm KS} = 0.031$, $P_{\rm KS} = 0.01 - 0.09$; Q0302−003: $d_{\rm KS} = 0.030$, $P_{\rm KS} = 0.02 - 0.11$; and Q0636+690: $d_{\rm KS} = 0.024$, $P_{\rm KS} = 0.09 - 0.31$. The ΛCDM$_{\rm H}$ model gives for Q0956+122: $d_{\rm KS} = 0.035$, $P_{\rm KS} = 0.003 - 0.04$. As was found for Q1937−1009 and HS 1946+7658 above, the ΛCDM$_{\rm L}$ and ΛCDM$_{\rm H}$ model predictions tend to bracket the measured distributions. The CHDM and tCDM models are strongly rejected by all the QSO spectra, even allowing for possible correlations in the pixel flux values.

3.3.2 Wavelet coefficient distributions

As for HS 1946+7658, the predicted model distributions for the wavelet coefficients are computed by extrapolating about the simulation results at $z = 3$, as this is closest to the redshift ranges of the spectra. The values for α from Table 4 are used in the extrapolation. The resulting wavelet coefficient distributions are displayed in Fig. 14. The agreement between the model predictions and the data is poor at the pixel scale (4–$8\,{\rm km\,s^{-1}}$). As was found in the previous QSO spectra, the data show a greater amount of structure. The data continue to show more structure on the 8–$16\,{\rm km\,s^{-1}}$ scale

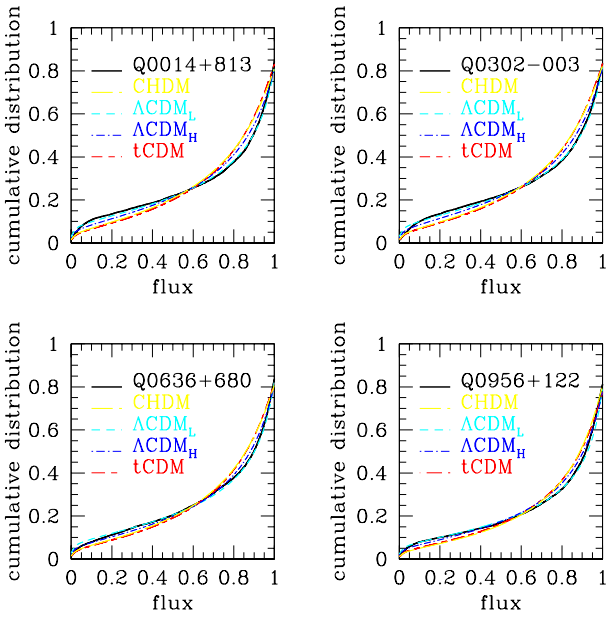

Figure 13. Comparison between the measured flux distributions of the Hu et al. (1995) QSO spectra and the model predictions. A continuum offset was applied to each model to enforce matching the predicted and measured cumulative distributions at flux values near unity. For all spectra except Q0956+122, the ΛCDM$_{\rm L}$ model provides the best match. For Q0956+122. the best match is given by the ΛCDM$_{\rm H}$ model.

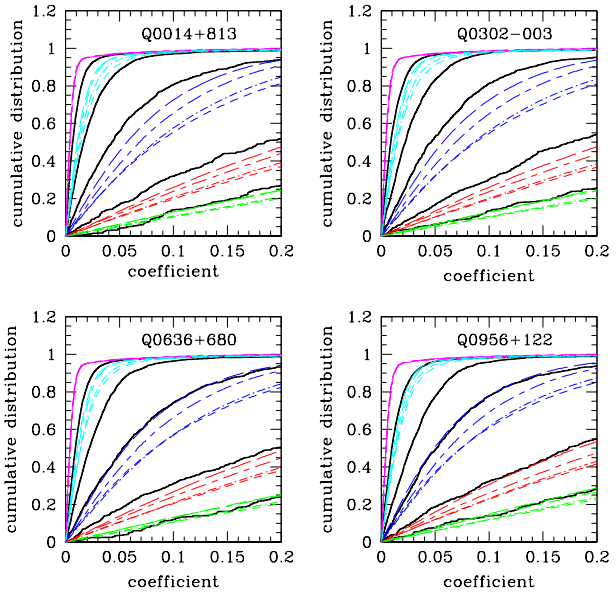

Figure 14. Comparison between the measured wavelet coefficient cumulative distributions of the Hu et al. (1995) QSO spectra (heavy solid curves) and the model predictions, allowing for continuum offset corrections. The curves from left to right correspond to the approximate velocity scales 4–8, 8–16, 16–32, 32–64, and 64–128 km s^{-1}. Model predictions are shown for CHDM (long-dash), ΛCDM$_{\rm L}$ (short dash), ΛCDM$_{\rm H}$ (dot – short dash), and tCDM (short dash – long dash). The best match for the velocity scale 16–32 km s^{-1}, corresponding to the median measured Doppler parameters, is found for the CHDM model in all cases. All the models underpredict the amount of structure on smaller velocity scales.

as well. Since the spectra resolve features on these scales, the differences appear to be physical. At the next level (16–32 km s^{-1}) the trend reverses: the models predict more structure than found in the data. The best agreement is consistently found for the CHDM model. The agreement, however, is statistically acceptable only for Q0636+680 and Q0956+122, according to the KS test. (For Q0636+680, $d_{\rm KS} = 0.018$, $P_{\rm KS} = 0.88$, and for Q0956+122, $d_{\rm KS} = 0.035$, $P_{\rm KS} = 0.17$.) The level of agreement shows significant scatter. The CHDM model predictions at 16–32 km s^{-1} agree well with the data for Q0636+680 and Q0956+122, but not for the remaining two QSOs. The CHDM model performs acceptably well on larger scales for all the QSOs.

3.3.3 Absorption line parameter distributions

The H I column density and Doppler parameter distributions derived by the AutoVP analyses of the QSO spectra of Hu et al. (1995) are shown in Figs 15 and 16 along with the model predictions. All the models predict an H I column density distribution and Doppler parameter distribution that both peak at lower values than measured. Of the four QSO spectra, the $N_{\rm HI}$ distribution for only Q0636+680 is well-represented by any of the models. The prediction of CHDM, the best-fitting model, for the $N_{\rm HI}$ distribution of Q0636+680 gives $d_{\rm KS} = 0.11$ and $P_{\rm KS} = 0.004$, while all other models are rejected. For all the remaining QSO spectra, CHDM provides the best match to the measured $N_{\rm HI}$ distribution as well, although the predicted distributions are rejected by the KS test.

None of the models provides an acceptable match to the measured b distributions, although the CHDM model consistently comes closest. As found for Q1937−1009 and HS 1946+7658, the model (ΛCDM$_{\rm L}$ or ΛCDM$_{\rm H}$) which best agrees with the measured flux per pixel distribution produces Doppler parameters that are too small. The measured median Doppler parameters (after removing metal lines, as discussed below), for Q0014+813, Q0302−003, Q0636+680, and Q0956+122 are, respectively, 30.5 ± 1.2 km s^{-1}, 29.5 ± 1.2 km s^{-1}, 26.1 ± 1.1 km s^{-1}, and 28.4 ± 1.3 km s^{-1}. The predictions of ΛCDM$_{\rm L}$ range between 17–18 km s^{-1} for all the QSOs, and for ΛCDM$_{\rm H}$ the prediction is 19 km s^{-1}, all too small by 35–75 per cent and by at least 6σ.

The AutoVP analysis of Q0636+680 produces 272 lines (after removing identified metal lines). The CHDM model predicts 334 lines, greatly in excess of the measured number. Similar or larger discrepancies between the predicted and measured number of absorption lines are found for all the QSO spectra and models, generally reflecting the narrowness of the predicted absorption features compared with the measured.

We note that Hu et al. (1995) report a significantly larger number of narrow absorption features in the spectrum of Q0636+680 than in any of the other spectra, and that most of these may be identified with metal lines (13 lines in the redshift range analysed here). They consequently

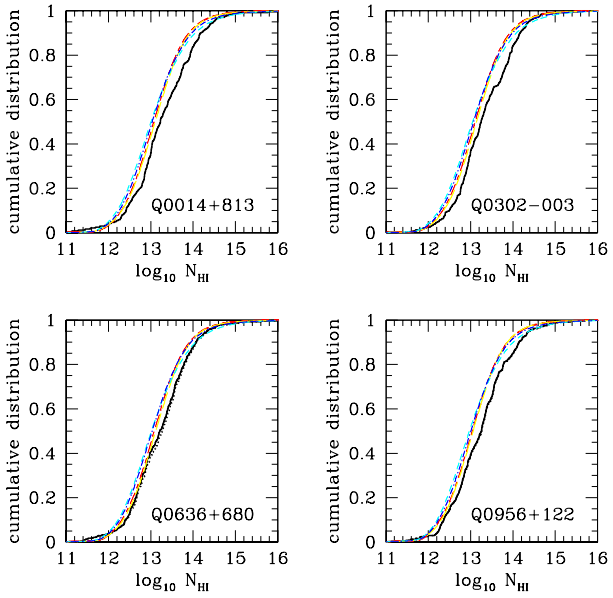

Figure 15. Comparison between the H I column density distributions measured using the Hu et al. (1995) QSO spectra and the model predictions. The curves are labelled as in Fig. 14. All the models predict a steeper distribution than measured. The dotted curves show the distributions after the removal of identified metal lines.

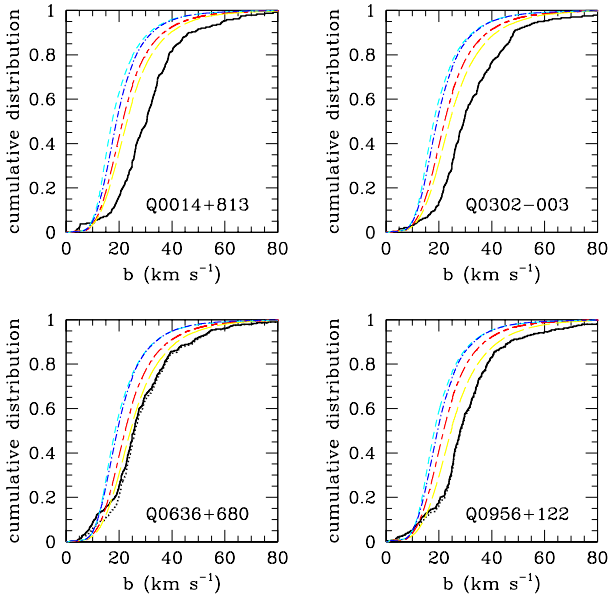

Figure 16. Comparison between the Doppler parameter distributions measured using the Hu et al. (1995) QSO spectra and the model predictions. The curves are labelled as in Fig. 14. All the models predict a distribution peaking at lower values than measured. The dotted curves show the distributions after the removal of identified metal lines.

exclude Q0636+680 from their statistics of the Lyα forest. We similarly find a larger number of narrow lines ($b < 10\,\mathrm{km\,s^{-1}}$) in Q0636+680 compared with the other spectra. We find that, based on the KS test, the flux and $N_{\rm HI}$ distributions show no anomalous behaviour compared with the other three spectra. In fact, these distributions, along with the b distribution, agree better with the model predictions than the distributions found for any of the other QSO spectra. The amount of metal line contamination based on the tabulations in Hu et al. (1995) is small (5 per cent of the lines in Q0636+680, 2 per cent in Q0956+122, no lines in Q0014+813 and 1 line in Q0302−003). Removing the narrow lines in the AutoVP analysis that most closely match the metal lines reported in Hu et al. (1995) has little effect on the $N_{\rm HI}$ and b distributions, as shown in Figs 15 and 16. Although some of the narrow absorption features remaining may still be unidentified metal lines, the similarity in the $N_{\rm HI}$ distributions between Q0636+680 and the other three QSOs suggests it is unlikely the contamination is large, so that it would seem unlikely that unidentified metal lines account for the large difference between the b distribution of Q0636+680 and the other three QSOs. Moreover, there is no statistically significant difference between the median Doppler parameters of the optically thin ($b_{\rm med} = 25.8 \pm 1.5\,\mathrm{km\,s^{-1}}$) and optically thick ($b_{\rm med} = 26.8 \pm 1.4\,\mathrm{km\,s^{-1}}$) systems in Q0636+680 (as is true for all the Hu et al. QSOs). If there were still substantial metal contamination present, a significantly larger median b-value for the optically thick systems may be expected. Because the median b-values of the optically thin and thick systems are consistent for each of the QSOs, the discrepancy between the predicted and measured Doppler parameters found may not be attributed predominantly to the optically thin systems, unlike the cases of Q1937−1009 and HS 1946+7658.

3.4 J2233−606

3.4.1 Flux distribution

The mean optical depth for J2233−606 is $\bar{\tau}_\alpha = 0.16$ over the analysis redshift interval $1.732 < z < 2.132$. The rescaling parameters used are given in Table 5. The simulation results at only $z = 2$ are used to extrapolate over the analysis redshift range, using the values for α from Table 4. It was found unnecessary to include any additional amount of evolution in the UV radiation background.

The distributions of flux per pixel are shown in Fig. 17. All of the models differ greatly from the data; the $\Lambda\mathrm{CDM_L}$ model is closest. Cristiani & D'Odorico (2000) have identified a large number of metal absorption features in the spectrum. The dotted line in Fig. 17 shows the flux distribution after removing regions of the spectrum within 2Å of an identified metal line. The effect is to worsen the agreement with the models. The reason for the poor agreement is unclear. At the low redshift of the QSO ($z_{\rm em} = 2.238$), the fundamental mode across the simulation volume is beginning to become non-linear. As a check, we have computed the flux per pixel distributions by extrapolating the optical depths from the simulation output at $z = 3$ to the redshift range of the spectrum. Nearly identical flux per pixel distri-

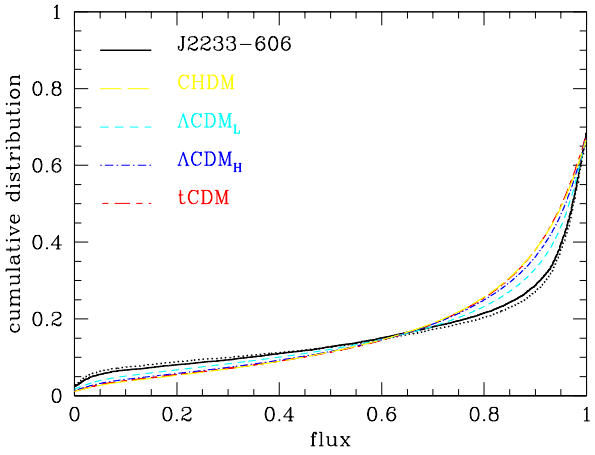

Figure 17. Comparison between the measured flux per pixel distribution of J2233−606 and the model predictions. A continuum offset was applied to each model to enforce matching the cumulative distributions at flux values near unity. None of the models recover the measured flux distribution, although the ΛCDM$_L$ model is closest. The dotted line shows the measured flux distribution after removing regions contaminated by identified metal lines.

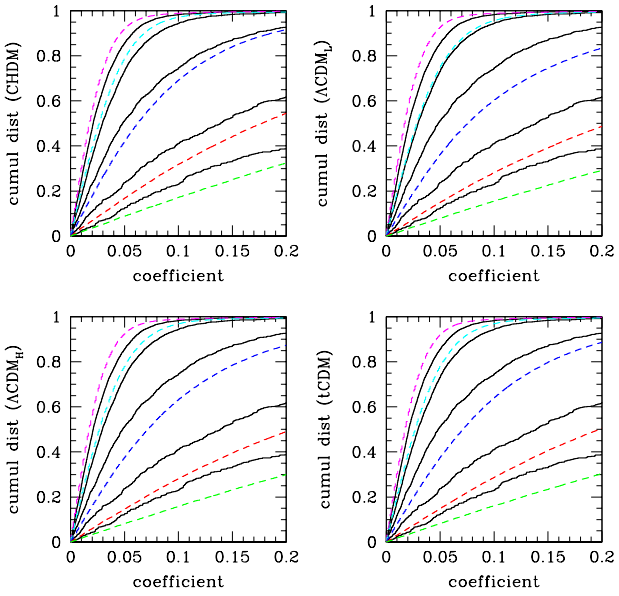

Figure 18. Comparison between the measured wavelet coefficient cumulative distributions of J2233−606 (solid curves) and the model predictions (dashed curves), allowing for continuum offset corrections. The curves from left to right correspond to the approximate velocity scales 4–7, 7–13, 13–27, 27–54, and 54–108 km s^{-1} . The best match for the velocity scale 13–27 km s^{-1} , corresponding to the median measured Doppler parameter, is found for the CHDM model. All the models underpredict the amount of velocity structure on smaller scales.

butions result, so that the disagreement appears not to be due to a lack of convergence in the simulation.

3.4.2 Wavelet coefficient distributions

The wavelet coefficient distributions are shown in Fig. 18. All the models poorly match the velocity structure on scales of 7–13 km s^{-1} and smaller. The best agreement on the 13–27 km s^{-1} scale, corresponding to the measured median Doppler parameter (see below), is provided by the CHDM model, although the match is rejected by the KS test ($d_{KS} = 0.09$, $P_{KS} = 10^{-9}$). The models recover the measured behaviour on larger velocity scales only moderately well to poorly.

3.4.3 Absorption line parameter distributions

Despite the poor agreement with the measured flux distribution, all the models well reproduce the N_{HI} distribution, as shown in Fig. 19. (Using the line list of Cristiani & D'Odorico (2000), we match 28 of the narrow lines found to identified metal lines and remove them.) The best agreement is given by the ΛCDM$_L$ model, with $d_{KS} = 0.078$ and $P_{KS} = 0.20$. The model predictions, however, disagree in the number of lines. The predicted numbers are for CHDM: 306, ΛCDM$_L$: 304, ΛCDM$_H$: 312, and tCDM: 327, all greatly in excess of the measured number of 192.

The model predictions for the b distributions agree poorly with that measured. The CHDM model agrees best,

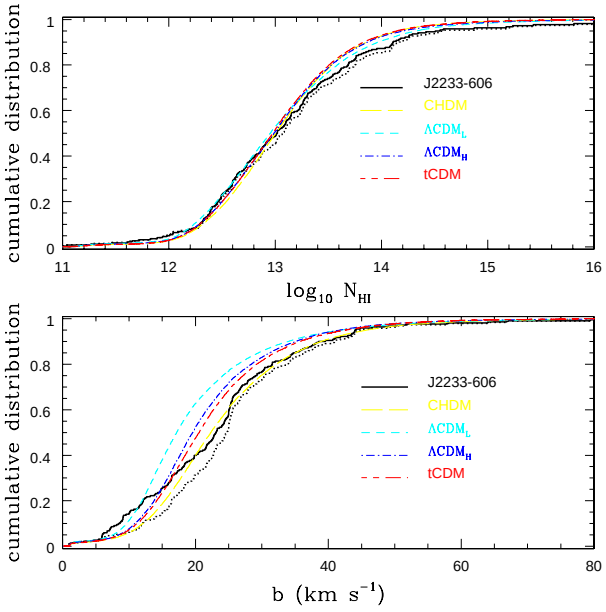

Figure 19. Comparison between the measured absorption line parameter distributions of J2233−606 and the model predictions. The dotted lines show the measured distributions once identified metal lines have been removed.

with $d_{\rm KS} = 0.13$ and $P_{\rm KS} = 0.004$. The predicted distributions of the remaining models are all strongly rejected. As was found for all the previous QSO spectra, the model ($\Lambda{\rm CDM_L}$) which provides the best match to the flux per pixel distribution underpredicts the measured median Doppler parameter. The measured median is $24.7 \pm 1.2\,{\rm km\,s^{-1}}$, while $\Lambda{\rm CDM_L}$ predicts $17.2\,{\rm km\,s^{-1}}$, too small by 6σ.

Splitting the sample into optically thin and optically thick systems tends to worsen the agreement for the $N_{\rm HI}$ predicted distributions of the optically thick absorbers to the point that they are only marginally acceptable (the best cases are CHDM and $\Lambda{\rm CDM_L}$, both with $d_{\rm KS} = 0.25$ and $P_{\rm KS} = 0.006$). The predicted $N_{\rm HI}$ distributions for the optically thin systems, however, all agree well with the measured (optically thin) distribution. Only the CHDM and tCDM models predict b distributions consistent with the measured for the optically thick absorbers (the tCDM prediction is marginal), while only the CHDM model predicts a b distribution consistent with the measured for the optically thin systems. The agreement for CHDM tends to improve for both the $\tau_0 < 1$ and $\tau_0 > 1$ subsamples compared with the full sample. The number of optically thick lines predicted by CHDM is 60, agreeing well with the measured number of 48. The number of optically thin lines, however, agrees poorly: the predicted number is 246, while only 144 are measured.

4 DISCUSSION

In this section we consider the possible systematics and limitations of each of the tests employed, and discuss what may still be concluded from the comparison between the models and the data. No single cosmological model clearly emerges as the best based on the full set of statistical tests. The measured distributions of flux per pixel are the most accurately reproduced, with the agreement reaching high precision. The agreement between the predicted and measured wavelet coefficients, however, is substantially poorer. The data generally show considerably less structure than the models predict on the velocity scale of approximately 15–30 ${\rm km\,s^{-1}}$. While the agreement often improves on larger velocity scales, the best–fitting models tend to be those that provide poor fits to the measured pixel flux distributions. The Voigt absorption line decompositions of the spectra similarly display a conflict: most of the models predict significantly narrower absorption features than measured, with the best agreement obtained by those models which agree most poorly with the measured flux per pixel distributions.

We show below that the shape of the flux per pixel distribution is sensitive to the amount of power in the models on small scales. The absorption properties of the spectra tend to be dominated by features that are marginally optically thick at line-centre ($13.5 < \log_{10} N_{\rm HI} < 14$), which are reproduced in the simulations by structures with filamentary morphologies (Miralda-Escudé et al. 1996; Zhang et al. 1998). The thicknesses of the filaments correspond to the scale height expected for photoionized gas in hydrostatic equilibrium within the gravitational potential of structures with a moderate cosmological overdensity (Zhang et al. 1998). For small density contrasts, this scale height is essentially the cosmological Jeans length of the gas. We shall show that the flux distributions produced by the absorbers vary systematically with the amount of power in the linear power spectra on these scales. In the linear theory of the gravitational growth of density fluctuations including baryons, the Fourier density modes of the baryons are suppressed by the factor $1/[1 + (k/k_{\rm J})^2]$, where $k_{\rm J} = (4\pi G\rho a^2)^{1/2}/c_s$ is the (comoving) cosmological Jeans wavenumber for a total cosmological density ρ and baryonic sound speed c_s, and a is the expansion factor (Peebles 1984, 1993). (The corresponding proper Jeans length is $L_J \equiv 2\pi a/k_J = 2\pi(2/3)^{1/2} c_s/H(z)$, where $H(z)$ is the Hubble constant at redshift z.) It is therefore useful to define the density fluctuations $\sigma_{\rm J}$ filtered on the scale $k_{\rm J}$ according to

$$\sigma_{\rm J}^2 = \int_0^\infty d\log k \frac{\Delta^2(k)}{[1 + (k/k_{\rm J})^2]^2}, \qquad (4)$$

where $\Delta^2(k)$ is the dimensionless power spectrum $k^3 P(k)/2\pi^2$ at the scale k. For simplicity, we define $\sigma_{\rm J}$ at $z = 3$, choosing c_s to be the isothermal sound speed $16.8\,{\rm km\,s^{-1}}$ for fully ionized gas at a temperature 2×10^4 K , the estimated temperature for gas with an overdensity near unity at $z = 3$ (McDonald et al. 2000a; Ricotti, Gnedin & Shull 2000; Schaye et al. 2000).

4.1 Flux distribution

The simulations are able to reproduce the measured flux per pixel distributions to extremely high accuracy. The best case is given by the SCDM model for Q1937−1009. The maximum difference between the measured and predicted cumulative flux distributions is $d_{\rm KS} = 0.016$, close to the level of precision of the simulation (see Appendix A). For HS 1946+7658, the $\Lambda{\rm CDM_H}$ model predicted distribution agrees with the measured to $d_{\rm KS} < 0.04$. Similar levels of agreement are found for the other QSO spectra examined, except for J2233−606 which appears anomalous.

Despite the close agreement between the predicted and measured flux distributions, the formal statistical acceptability of the matches, as given by the KS test, is generally poor. This is in part due to the large number of pixels involved (approximately 10^4), which permits a stringent comparison to be made. It is, however, also due to deviations from the theoretical KS probability distribution of $d_{\rm KS}$. In practice, the probability distribution is broader than the theoretical, which is likely a consequence of correlations between neighbouring pixel flux values (see Appendix A). Allowing for the correlations to decrease the effective number of degrees-of-freedom yields acceptable agreement for the predicted distributions of either the $\Lambda{\rm CDM_L}$ or $\Lambda{\rm CDM_H}$ model (or both) for all the QSOs (except HS 1946+7648, although the predicted distributions of the two ΛCDM models bracket the measured distribution, and J2233+606), while the predictions of the CHDM and tCDM models are consistently rejected. We note that Rauch et al. (1997) and McDonald et al. (2000b) also found very close agreement between the predicted flux distribution of a ΛCDM model similar to our $\Lambda{\rm CDM_H}$ model and the measured flux distribution in a set of QSO spectra observed with the Keck HIRES. In contrast to our results, however, Rauch et al. found the predicted flux distribution of an SCDM model nearly identical to ours to agree less well with the measured.

The flux distributions are found to vary systematically with $\sigma_{\rm J}$, the density fluctuations on the scale of the cosmological Jeans length. As shown in Fig. 3, as $\sigma_{\rm J}$ increases, the distributions flatten (as measured between flux values of 0.2 and 0.8). This is similar to the trend found by M00 of increasing width of the probability distribution of $\log\tau$ with increasing small-scale power. The best-fitting predicted flux distribution for Q1937−1009 is provided by the SCDM model, for which $\sigma_{\rm J} = 1.6$. Although the predicted flux distributions of the $\Lambda{\rm CDM_L}$ and $\Lambda{\rm CDM_H}$ models agree less well, their cumulative flux distributions bracket the measured distribution, as is found for all the QSO spectra except J2233+606. The values of $\sigma_{\rm J}$ for these models (1.7 and 1.3, respectively), similarly bracket the value of $\sigma_{\rm J}$ for the SCDM model, so that it is reasonable to expect a ΛCDM model with an intermediate value of $\sigma_{\rm J}$ would provide a better fit.

The success of the ΛCDM models in predicting pixel flux distributions that bracket the measured distributions suggests a strong bound on the small scale power of the primordial power spectrum at $z = 3$ of $1.3 < \sigma_{\rm J} < 1.7$ (with greater than 3σ certainty). This result combined with limits on $\sigma_{8h^{-1}}$ from cluster abundances (Pierpaoli et al. 2001), on the primordial power spectrum shape parameter ($0.19 < \Gamma_{\rm PS} < 0.37$; Eisenstein & Zaldarriaga 2000) and its amplitude (Bunn & White 1997) and spectral index ($0.9 < n < 1.1$; Netterfield et al. 2001; Pryke et al. 2001; Stompor et al. 2001), imposes the limit on the cosmological matter density $0.26 < \Omega_M < 0.43$ for a flat universe ($\Omega_\Lambda = 1 - \Omega_M$), and assuming $\Omega_b h^2 = 0.020$ (O'Meara et al. 2000), $0.45 < h < 0.85$, and no massive neutrino species. These restrictions ease somewhat to $0.26 < \Omega_M < 0.68$ if up to two massive neutrino species are allowed accounting for a total mass fraction $\Omega_\nu \leq 0.2$, and the 3σ limits of Pierpaoli et al. (2001) are permitted. These limits are in good agreement with those found elsewhere (eg, Netterfield et al. 2001; Pryke et al. 2001; Stompor et al. 2001). Adopting $\Gamma_{\rm PS} = 0.15$ in accordance with Croft et al. (2000), based on the flux power spectrum $P_F(k)$ measured in several Lyα forest spectra, gives (for $1.3 < \sigma_J < 1.7$) the limits $0.23 < \Omega_M < 0.45$ ($\Omega_\Lambda = 1 - \Omega_M$, $\Omega_\nu = 0$), in satisfactory agreement with the limits of Croft et al. (2000).

4.2 Evolution of Γ

Since the gas is in photoionization equilibrium, the optical depth in Lyα is predicted by the models only to within the factor $b_{\rm ion}$ (§ 3). The re-normalizations of the optical depths required for a given model to match the measured mean optical depth in Lyα of a QSO spectrum provides an estimate of the value of Γ required.

In Figure 20 we show the required values of Γ for the models to match the measured mean optical depth $\bar\tau_\alpha$ in each QSO spectrum. The width of a given horizontal bar indicates the redshift range analysed in the QSO spectrum, and the corresponding point marks the required value of Γ at the central redshift. Two estimates are made. For the first, we show the values of Γ assuming the value for Ω_b adopted in each model. For the second, we show the values of Γ assuming $\Omega_b h^2 = 0.020$ (O'Meara et al. 2000) after rescaling the optical depths by $b_{\rm ion}$. The scatter is considerably reduced

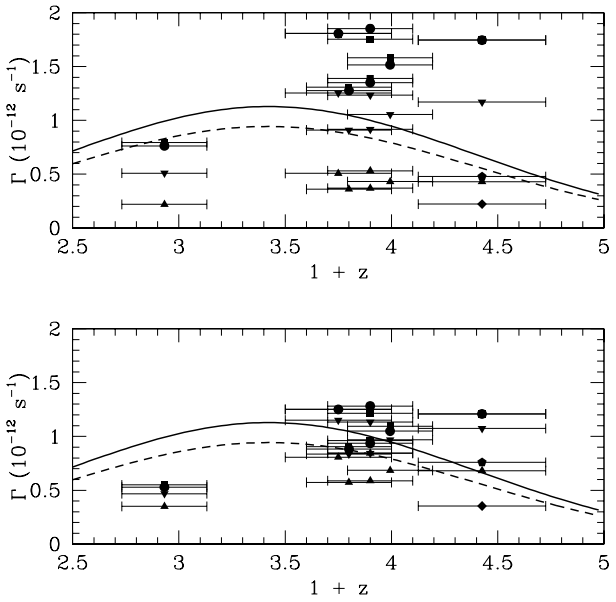

Figure 20. Required H I photoionization rate Γ required for the models to match the measured mean optical depths, for CHDM (circles), $\Lambda{\rm CDM_L}$ (triangles), $\Lambda{\rm CDM_H}$ (inverted triangles), tCDM (squares), OCDM (diamonds), and SCDM (pentagons). The upper panel shows Γ for the value of Ω_b assumed in the model. The lower panel shows Γ assuming a fixed value of $\Omega_b h^2 = 0.020$ for all the models. The predicted values are close to the estimated Γ from QSO sources alone for an intrinsic QSO spectral index of $\alpha_Q = 1.5$ (solid curve) and $\alpha_Q = 1.8$ (dashed curve).

in the latter case. Also shown are the theoretical predictions for Γ due to QSO sources alone, assuming an intrinsic QSO spectral index of $\alpha_Q = 1.5$ or 1.8 (Haardt & Madau 1996). The required values of Γ are found to lie within a factor of 2 of the predicted rates for $\Omega_b h^2 = 0.020$, suggesting little, if any, sources additional to QSOs are required, or are even permitted without destroying the agreement between the models and the measured spectra. We note, however, that the rate of evolution of Γ necessary to match the measurements of the mean optical depth over the redshift range probed by the spectrum of Q1937–1009 ($3.1 < z < 3.7$) was found to be significantly slower than given by Haardt & Madau (1996). The difference may be due to the uncertainty in the QSO counts at these high redshifts.

The values we obtain for Γ for the $\Lambda{\rm CDM_H}$ model at $z = 3$ is about twice that reported by McDonald et al. (2000b) for a very similar model. (Here and below, we use $b_{\rm ion}$ to re-normalize the reported values of Γ to $\Omega b^2 = 0.020$.) The difference is likely due primarily to the larger value for $\bar\tau_\alpha$ they find. Our results are in closer agreement with those of Rauch et al. (1997) in the redshift intervals $2.5 < z < 3.5$ and $3.5 < z < 4.5$, although our values for Γ still lie somewhat higher. By contrast, our value for Γ for the SCDM model in the interval $3.1 < z < 3.7$ is about a factor of 2 below that found by Rauch et al. for SCDM in the range $3.5 < z < 4.5$. The difference may in part stem from an overestimate of $\bar\tau_\alpha$ by the SCDM model simulation used by

Rauch et al. (that of Croft et al. 1997), as was demonstrated by Theuns et al. (1998b). The value for Γ reported by Weinberg et al. (1997) at $z = 3$ is just above the spread of values we find for our various models.

4.3 Wavelet coefficient distributions

The wavelet coefficient distributions predicted by the models show considerable disagreement with the measured distributions. The deviations are greatest on the velocity scale of approximately 15–30 $\mathrm{km\,s^{-1}}$, with the models generally predicting a much greater amount of structure than is found in the data. The closest agreement is found for the CHDM model on this scale for all the QSO spectra. The CHDM model predicts distributions on this scale consistent with the data for Q1937−1009 and HS 1946+7658. The level of agreement, however, is inconsistent among the Hu et al. (1995) QSOs on the 16–32 $\mathrm{km\,s^{-1}}$ scale. While good agreement is found for Q0636+680 and Q0956+122, the CHDM predictions are strongly rejected by the KS test for Q0014+813 and Q0302−003.

To investigate the reasons for the inconsistency in the level of agreement on the 16–32 $\mathrm{km\,s^{-1}}$ scale of a given model among the various Hu et al. QSO spectra, we compare the measured wavelet distributions of these spectra. A comparison of the distributions of Q0302−003 and Q0636+680 shows that they are only marginally consistent on the 16–32 $\mathrm{km\,s^{-1}}$ scale ($d_{\mathrm{KS}} = 0.08$, $P_{\mathrm{KS}} = 0.005$) (while consistent on the other scales examined). A comparison between Q0302−003 and Q0956+122, however, shows the distributions to be consistent on the scale of 16–32 $\mathrm{km\,s^{-1}}$ and higher, but not on smaller scales. The data show statistically significant inhomogeneity. For this reason, we have chosen to treat the analyses of the QSOs separately. (We note that the flux per pixel distributions of the four Hu et al. QSO spectra show no significant differences over the analysis redshifts, and so in principle could have been treated together. For uniformity of presentation, we compare the numerical results with the results from each spectrum individually as well.)

The level of agreement between the models and the data is not much improved on the next smaller scale of approximately 8–16 $\mathrm{km\,s^{-1}}$. While the predicted distributions of coefficients for Q1937−1009 tend to scatter either above or below the measured, the predicted coefficients are systematically too small on this scale for HS 1946+7658. The additional measured structure in the latter spectrum may reflect the large number of metal absorption lines identified (Kirkman & Tytler 1997), which will give rise to features on this scale.

None of the models reproduce the light fluctuations on the pixel scale, as determined by the lowest level wavelet coefficients. It may be that the disagreement results from limitations of the simulations. For an expansion velocity difference across the simulation box at $z = 3.5$ of $\sim 1000\,\mathrm{km\,s^{-1}}$ and 256 grid zones along a side, the characteristic velocity resolution is $\sim 4\,\mathrm{km\,s^{-1}}$, so that it may be difficult to reproduce fluctuations in the spectra on these scales.

Although the wavelet analysis provides a quick and precise means of comparing the model predictions with the data, it has the disadvantage of not directly relating any discrepancies to physical quantities. Larger (or smaller) measured coefficients than predicted at a given velocity scale will arise because fewer (or more) absorption systems are predicted by the model on this scale, but the wavelet coefficients alone cannot determine whether this is a consequence of a mismatch of the density fluctuation spectrum, the assumed cosmological model, the presence of contaminating lines (metal systems), or the thermal properties of the gas. To examine these issues, we also perform a Voigt absorption line analysis.

4.4 Absorption line parameter distributions

The shapes of the predicted and measured H I column density distributions tend to accord well, though not perfectly. The AutoVP analysis of Q1937−1009 yields agreement with the measured N_{HI} distribution only for the CHDM model, and even this is marginal. The analysis of HS 1946+7658 (after removing identified metal lines) favours instead the ΛCDM models, although marginal agreement is again found for CHDM and tCDM. The predicted and measured N_{HI} distributions for all the Hu et al. (1995) spectra tend not to agree at an acceptable level, though the predictions of CHDM are favoured. The agreement with the N_{HI} distribution measured in J2233−606, however, is acceptable for all the models. The level of agreement is somewhat sensitive to the analysis method: better agreement is found for Q1937−1009 between the predicted and measured N_{HI} distributions using SPECFIT than AutoVP, though still at a marginal to poor level, except for $\Lambda\mathrm{CDM_L}$ for which the agreement is good. Of greater concern is the number of absorption systems found: both the AutoVP and SPECFIT analyses predict numbers of features inconsistent with the numbers measured.

Splitting the absorption line samples into subsamples optically thin and thick at the Lyα line-centre reveals that the discrepancies originate primarily from the optically thin systems. Acceptable agreement is found for the optically thick systems between the predicted and measured N_{HI} distributions for Q1937−1009 for all the models using AutoVP. (The agreement tends to worsen for SPECFIT, however, again suggesting that caution should be exercised in judging the viability of a model on the basis of the N_{HI} distribution alone.) The predicted and measured distributions for HS 1946+7658 for the optically thick systems coincide extremely closely for all the models examined, and acceptable agreement is again obtained for J2233−606 (though at a more marginal level). There is generally acceptable agreement between the predicted and measured numbers of optically thick absorbers as well.

The measured and predicted N_{HI} distributions for the optically thin systems match much more poorly. While excellent agreement is found between the predictions of the CHDM and tCDM models and the measured distribution in Q1937−1009 using AutoVP, all the other models are strongly rejected. (The SPECFIT analysis results in no acceptable models, though tCDM is marginal.) Poorer agreement is found for HS 1946+7658 among the optically thin systems than the optically thick as well, although the ΛCDM models are still acceptable. For J2233−606, the agreement with CHDM and tCDM is excellent, while the ΛCDM models are marginal.

We note that our results are somewhat at variance with those of Gnedin (1998), who uses a pseudo-hydrodynamical numerical technique to test a variety of cosmological models based on the predicted H I column density distributions. Gnedin finds acceptable agreement between the predictions of several models for the shape of the $N_{\rm HI}$ distribution with the tabulated distribution of Hu et al. (1995). By contrast, we find none of our models recovers the Hu et al. distribution, including our ΛCDM models which are very similar to models Gnedin finds acceptable. Based on the results of several models, Gnedin places 2σ and 3σ constraints on the size of density fluctuations for wavenumbers twice the Jeans wavenumber. Using his conversion formula to σ_{34}, the density fluctuations gaussian smoothed on the scale $k_{34} = 34\Omega_M^{1/2} h\,{\rm Mpc}^{-1}$, where Ω_M is the total matter density parameter, and the "effective equation of state" parameters reported by Ricotti et al. (2000), these limits become ($z = 2.85$) $1.4 < \sigma_{34} < 2.6$ (2σ) and $1.3 < \sigma_{34} < 3.1$ (3σ). These rule out our CHDM model ($\sigma_{34} = 1.4$) at the 2σ level and our tCDM model ($\sigma_{34} = 1.1$) at the 3σ level, but not the others. Yet we find that the shapes of the $N_{\rm HI}$ distributions predicted by CHDM and tCDM for Q1937−1009 (restricted to the optically thick systems, corresponding approximately to the column density range used by Gnedin in the same redshift range), are consistent with the measured (optically thick) distribution, with the CHDM model providing the best match of all the models. These two models also fare no worse than the others in comparison with the Hu et al. (1995) data, and often provide the best (though usually unacceptable) match to the measured $N_{\rm HI}$ distribution. Whether the disagreement between our findings and Gnedin's is due to differences in the absorption line analysis approaches or the simulation methods (Meiksin & White 2001) is unclear.

A much larger discrepancy is found between the measured Doppler parameter distributions and the distributions predicted by the simulations. The median measured Doppler parameters generally exceed the predicted by as much as 30–60 per cent. The best agreement is consistently found for the predictions of the CHDM model, although this model provides a poor match to the measured flux per pixel distributions. The next best match to the measured b distributions is provided by tCDM, which also predicts flux per pixel distributions in disagreement with the data. On the other hand, the models that match the measured pixel flux distributions predict Doppler parameters that are much too small. There appears no simple remedy to this conflict.

Splitting the sample into optically thick and optically thin absorbers at the Lyα line-centre shows that the discrepancy in the Doppler parameters is sensitive to the line-centre optical depth τ_0. The discrepancy in the measured and predicted Doppler parameters has been recognized for optically thick systems for ΛCDM, OCDM, and SCDM models (Theuns et al. 1998b; Bryan et al. 1999; Theuns et al. 1999; Bryan & Machacek 2000; M00). The results of M00, however, suggest that the discrepancy may be model-dependent, as the tCDM model was found there to provide reasonably good agreement. Here we find that the tCDM model provides an excellent match to the measured b distributions for the optically thick absorbers in Q1937−1009 and HS 1946+7658, while the b distributions predicted (for $\tau_0 > 1$) by the CHDM and $\Lambda{\rm CDM_H}$ models are consistent with that of HS 1946+7658, though not of Q1937−1009.

None of the models matches the distributions measured in the Hu et al. (1995) QSO spectra, although the CHDM model comes close for Q0636+680. This latter point is of particular concern, since previous model comparisons have been based on the Hu et al. QSO sample, supplemented by several other QSO spectra (Kim et al. 1997), but with Q0636+680 *excluded*. The reason for excluding it was the relatively large number of absorption features found, as well as the large number of metal systems identified in the spectrum: it appeared that the spectrum may be excessively contaminated by metal lines. We perform a comparison between the AutoVP results for Q0636+680 and the combined other three QSOs of Hu et al. over the common redshift range $2.7 < z < 3.0$ (with identified metal lines removed), and confirm a statistically significant difference in the b distributions using the KS test ($d_{\rm KS} = 0.16$, $P_{\rm KS} = 6\times10^{-4}$). The $N_{\rm HI}$ distributions, however, agree extremely well, which may not have been expected if a large amount of metal contamination was still present in the Q0636+680 line list. (The distributions of restframe equivalent widths and line-centre optical depths also agree extremely well.) The larger number of lines in Q0636+680 is expected given the relative narrowness of the features (in order to recover the measured value of $\bar{\tau}_\alpha$). Since all the spectra probe large cosmological distances ($\Delta z/(1+z) \approx 0.1$), sample variance would appear an unlikely explanation for the discrepancy in b-values. The smaller median b-value measured in Q0636+680 is also in better agreement with the median b-value measured in HS 1946+7658, at only a slightly smaller redshift. We conclude that there is little justification for preferring the results of the other Hu et al. QSO spectra over those of Q0636+680. Adopting the tabulated results of Hu et al. (1995) or Kim et al. (1997) as the fiducial b distribution for comparison with the simulation predictions may exaggerate the true level of disagreement, if any.

More pronounced disagreement in the Doppler parameters is found for the optically thin absorbers. Only the CHDM model is able to produce a distribution consistent with any of those measured (only for HS 1945+7658 and J2233−606, although the SPECFIT results of the CHDM model for Q1937−1009 are marginal). The discrepancy in the numbers of absorption systems is least for the CHDM model. This may be attributed to the larger b-values: fewer broader lines are required to produce the same mean optical depth $\bar{\tau}_\alpha$. A similar explanation accounts for the better agreement in the wavelet coefficient distributions compared with the other models on the scale of 16–32 $\rm km\,s^{-1}$: fewer features on this scale are produced by the CHDM model than by the other models, resulting in a smaller proportion of large coefficients and so a better match to the measured distributions.

Possibly a compromise cosmological model may be found which fits all the distributions. Increasing the baryon density will increase the temperature of the moderate density gas and hence the Doppler parameters (Meiksin 1994; Theuns et al. 1998b). For instance, doubling the baryon density for $\Lambda{\rm CDM_L}$ from $\Omega_b h^2 = 0.015$ to 0.03 would increase the gas temperature by 40 per cent, using the temperature-baryon density scaling of Zhang et al. (1998). This may increase the median Doppler parameter by as much as 10–

20 per cent, depending on the contribution of peculiar velocity broadening to the line widths (Zhang et al. 1998). Although such a high baryon density contradicts the deuterium abundance determinations of O'Meara et al. (2000) within the context of standard Big Bang Nucleosynthesis, it is consistent with reported CMB measurements of the acoustic peaks (Netterfield et al. 2001; Pryke et al. 2001; Stompor et al. 2001).

There is an issue of convergence of the simulation results, particularly for the b distribution. Theuns et al. (1998b) and Bryan et al. (1999) show that the b-values tend to decrease with increasing spatial resolution of the simulations, although they were able to explore the trend only for a limited range of box sizes. Meiksin & White (2001) expanded the box size and resolution ranges by performing pseudo-hydrodynamical N-body simulations of the Lyα forest. They found that convergence was particularly difficult to achieve in the distribution of wavelet coefficients on the scale of $16-32\,\mathrm{km\,s^{-1}}$ and in the b distribution. The results of their Particle-Mesh simulations suggest that the cumulative distributions may be determined only up to an absolute precision of $0.05-0.1$, and the convergence does not always scale monotonically with resolution. The convergence behaviour, however, was found to improve when a pseudo-pressure force was added, and so may be better for a full hydrodynamics computation as well. They were still unable to reach convergence in the cumulative b distribution to better than an absolute precision of about 0.05 even in the pseudo-pressure force case, and allowing for as many as 512^3 grid zones to compute the gravity, a greater number than used in the simulations here. The question of convergence of the full hydrodynamics simulations to an absolute precision of better than 0.05 in the cumulative b distribution we consider as yet unresolved. The general tendency, however, is to reduce the Doppler parameters at increased resolution, so that the discrepancy between the measured and predicted Doppler parameters is unlikely to result from a lack of convergence in the simulations.

Another possibility is that there is missing physics in the simulations. Late He II reionization will produce an increase in the temperature of the gas (Meiksin 1994; Miralda-Escudé & Rees 1994; Haehnelt & Steinmetz 1998; Abel & Haehnelt 1999). The possibility of late He II reionization, at a redshift of $z_{\rm HeII}=3-3.5$, has been suggested in a variety of contexts: on the basis of intergalactic He II optical depth measurements compared with H I (Madau & Meiksin 1994; Reimers et al. 1997); an abrupt change in the ionization parameter of metal lines at these redshifts (Songaila & Cowie 1996, but this has been disputed by Boksenberg, Sargent, & Rauch 1998); and determinations of an "effective equation of state" of the IGM (McDonald et al. 2000a; Ricotti et al. 2000; Schaye et al. 2000). Since the optically thin absorption originates preferentially in underdense regions (Zhang et al. 1998), these systems will not achieve thermal balance between photoionization heating and radiative cooling, and so will more strongly manifest the thermal effects of late He II ionization (Meiksin 1994). Since the associated heating will occur while the gas is out of ionization equilibrium, the temperature will be boosted by as much as a factor of 2 over the equilibrium case (Meiksin 1994). The low density optically thin absorbers will thereafter cool largely through adiabatic expansion, while the temperature of the higher density gas will relax from its post-photoionization level to a lower value as a result of radiative losses.

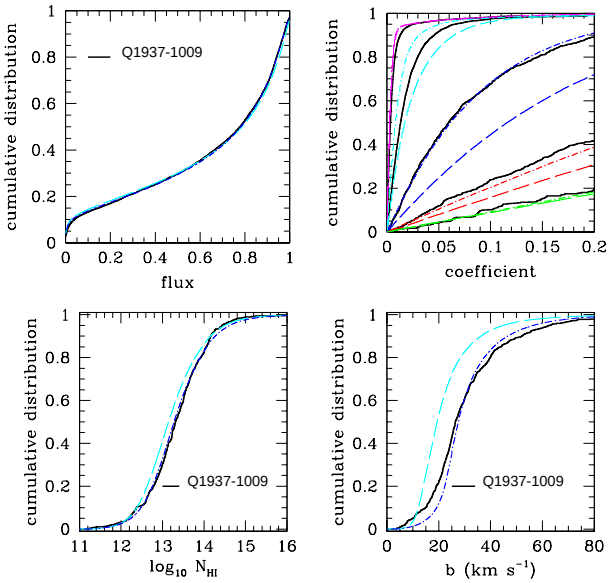

Figure 21. The effect of additional heat input due to late He II reionization on the predictions of the ΛCDM$_{\rm L}$ model for Q1937−1009. Shown are the cumulative distributions of the flux per pixel (top left panel), wavelet coefficients (top right panel; labelled as in Fig. 4), H I column density (bottom left panel) and Doppler parameter (bottom right panel). The effect of late reionization is mimicked by broadening the simulation optical depths by an additional $12\,\mathrm{km\,s^{-1}}$ (dot-dashed lines), corresponding to the expected increase in temperature due to the onset of sudden He II reionization. The original results without the added broadening are also shown (dashed curves), as well as the direct measurements from the spectrum of Q1937−1009 (solid curves). The extra broadening has very little effect on the flux per pixel distribution, but pronounced effects on the wavelet coefficients and fit absorption line parameters.

We may estimate the change in temperature immediately following He II photoionization as follows. Prior to He II ionization, the total number density of particles n_p is related to the number density of hydrogen nuclei $n_{\rm H}$ by $n_p=2(1+\xi)n_{\rm H}$, where $\xi=0.25Y_{\rm He}/(1-Y_{\rm He})$ is the ratio of helium nuclei to hydrogen nuclei, and the baryonic mass fraction of helium is $Y_{\rm He}=0.24$ (Izotov & Thuan 1998). (We have assumed that virtually all the helium is in the form of He II .) For a gas temperature T, the thermal energy density of the IGM is then $\epsilon_T=3(1+\xi)n_{\rm H}kT$, where k is the Boltzmann constant. After He II ionization, $n_p=(2+3\xi)n_{\rm H}$, and the thermal energy density will be $\epsilon'_T=(3/2)(2+3\xi)n_{\rm H}kT'$, where T' is the gas temperature immediately following reionization. For a He II heating rate $G_{\rm HeII}$ per He II ion and photoionization rate $\Gamma_{\rm HeII}$, the difference in thermal energies is $n_{\rm H}\xi G_{\rm HeII}/\Gamma_{\rm HeII}=\epsilon'_T-\epsilon_T$ for (nearly) complete reionization. The increase in temperature is then

$$\Delta T=T'-T\simeq\frac{1}{3k}\xi\frac{G_{\rm HeII}}{\Gamma_{\rm HeII}}=\xi\eta_{\rm HeII}\frac{\mathcal{E}_{\rm HeII}}{3k}, \qquad (5)$$

assuming $2\Delta T >> \xi T'$ and $\xi << 1$. The heating per ionization efficiency $\eta_{\rm HeII} \equiv G_{\rm HeII}/(\Gamma_{\rm HeII}\mathcal{E}_{\rm HeII})$, where $\mathcal{E}_{\rm HeII} = 54.4\,{\rm eV}$ is the ionization potential of He II , is sensitive to the spectral shape of the ionizing radiation field, which will harden within the ionization front, since higher energy photons will travel further than lower energy photons before being absorbed. This results in a boost in $\eta_{\rm HeII}$, and an increase in ΔT. We find for a radiation field intensity $J_\nu \propto \nu^{-\alpha}$ within the ionization front that $0.35 < \eta_{\rm HeII} < 1.1$ for $2 > \alpha > 0$. Assuming a hard field with $\alpha \approx 0$ gives $\eta_{\rm HeII} \approx 1$ and $\Delta T \approx 1.7 \times 10^4\,{\rm K}$.

We estimate the effects of an increase in temperature by broadening the optical depths in the $\Lambda{\rm CDM_L}$ simulation by convolving with a gaussian of effective velocity dispersion σ_T. (It may be argued that since the simulation already incorporates He II heating, a smaller temperature increase should be adopted. On the other hand, the value for $\Omega_b h^2$ is smaller than the estimate of O'Meara et al. (2000), so that the gas temperature of the moderate density gas is too low, which partially offsets the additional heating. In any case, the estimate is only approximate, since it does not account for the density dependence of the post-photoionization temperature or any dynamical changes that will result from the associated sudden change in thermal pressure.) The smoothing formally broadens the Doppler widths according to $b' = (b^2 + 2\sigma_T^2)^{1/2}$, where b and b' are the Doppler parameters prior to and just after the temperature increase ΔT, respectively. We find that $\sigma_T = 12\,{\rm km\,s^{-1}}$, corresponding to $\Delta T = 1.7 \times 10^4\,{\rm K}$, provides adequate broadening. The broadening results in a slight increase in $\bar\tau_\alpha$, requiring an increase in Γ to $5 \times 10^{-13}\,{\rm s^{-1}}$ (or $8 \times 10^{-13}\,{\rm s^{-1}}$ re-normalizing to $\Omega_b h^2 = 0.020$ using $b_{\rm ion}$) at $z = 3.5$ to match the measured value of $\bar\tau_\alpha$, in good agreement with the estimate of Haardt & Madau (1996). We allow for this increase (corresponding to a reduction in s in Table 3 from 2.56 to 2.1) when re-synthesizing the model spectra. We show in Fig. 21 the effects of the broadening on the flux per pixel distribution, wavelet coefficients, and absorption line parameters after synthesizing spectra to match that of Q1937−1009, using the same procedure as previously. The KS test comparisons with Q1937−1009 show excellent agreement with the distributions of flux per pixel ($d_{\rm KS} = 0.018$, $P_{\rm KS} = 0.003$ assuming fully independent pixels, and $P_{\rm KS} = 0.23$ assuming a reduction by a factor of 3 in their effective number), the wavelet coefficients on the scale of 17–34 ${\rm km\,s^{-1}}$ ($d_{\rm KS} = 0.023$, $P_{\rm KS} = 0.50$) and higher, and the $N_{\rm HI}$ distribution ($d_{\rm KS} = 0.044$, $P_{\rm KS} = 0.28$). Poor agreement is found for the lower velocity wavelet coefficients and the b distribution because of excessive smoothing on small velocity scales. The predicted median b-value ($b_{\rm med} = 27.6\,{\rm km\,s^{-1}}$), however, now matches the measured.

We remark that the additional smoothing has only a small effect on the pixel flux distribution, bringing it into slightly better agreement with the measured. Much larger effects are produced on the light fluctuations, as quantified by the wavelet coefficients and absorption line parameters. While previously the predicted $N_{\rm HI}$ distribution for the $\Lambda{\rm CDM_L}$ was strongly rejected by the KS test for Q1937−1009, it now provides an excellent match. The predicted number of absorption lines (453) now also agrees with the measured number (495). The decrease in number is a direct consequence of the broadening of the lines, as is the good match in the wavelet coefficients and the improved match in the Doppler parameters. The shape of the $N_{\rm HI}$ distribution, the number of absorption lines, the wavelet coefficients and the b-values are all linked, changing together in response to the broadening of the absorption features. We see, then, that it is because the CHDM model produces broader lines than the other models that it (usually) provides the best match to these distributions. We caution that conclusions drawn on the basis of any one of these distributions alone are thus precarious: if one of the distributions is poorly matched, whatever fixes it will alter the others. By contrast, the flux per pixel distribution is much less sensitive to changes in the widths of the absorption features, and thus provides a much more robust test of the cosmological model.

An alternative explanation for the broader measured lines compared with the model predictions may be galactic feedback. One possibility is Compton heating by Active Galactic Nuclei (Madau & Efstathiou 2000). Although Bryan & Machacek (2000) found the heating rate inadequate, this may only be a reflection of the particular parameters adopted for the rate and its evolution. Another possibility is heating or turbulent broadening by galactic winds. The possible role of galactic winds in enriching the IGM with metals has been considered by several authors (Wang 1995; Nath & Trentham 1997; Ferrara, Pettini & Shchekinov 2000; Madau, Ferrara & Rees 2000; Aguirre et al. 2001; Theuns, Mo & Schaye 2001). As part of the metal-enrichment process, winds from forming galaxies will inject energy into their surroundings. Although the temperature of the remnant wind material will decline with time after the winds cease (Madau et al. 2000), the galactic winds associated with ongoing star-formation will provide a continuous source of energy to the IGM, broadening the absorption lines either thermally or through turbulence driven by dynamical instabilities. Whether or not this is possible without severely disturbing the agreement with the $N_{\rm HI}$ distributions is unclear, but we may consider the energetics required to alter the Doppler parameter distribution. We estimate the energy density of the Lyα forest as follows. The combined thermal and kinetic energy per particle in gas giving rise to an absorption feature with a Doppler parameter b is on the order of $\epsilon_p \approx (3/4) m_{\rm H} b^2$, where $m_{\rm H}$ is the mass of a hydrogen atom. Half the baryons are contained in Lyα absorption systems with $13 < \log_{10} N_{\rm HI} < 15$ at $2 < z < 4$ (Miralda-Escudé et al. 1996; Zhang et al. 1998). For an *rms* Doppler parameter of $b \approx 25\,{\rm km\,s^{-1}}$, this gives a total (proper) energy density in the Lyα forest at $z = 3$ of $\epsilon_{{\rm Ly}\alpha} \approx 5 \times 10^{-17}\,{\rm erg\,cm^{-3}}$. An increase in the Doppler parameter by 20 per cent would require an increase in the energy density by 40 per cent. We compare this with the possible amount of energy injected by supernovae. For a (proper) cosmic star formation rate density at $z > 3$ of $1 - 10\,{\rm M_\odot\,yr^{-1}\,Mpc^{-3}}$ (Madau et al. 1996; Steidel et al. 1999; Rhoads et al. 2001) that has been ongoing for $\sim 10^9\,{\rm yr}$, a supernova rate of 1 per $100\,{\rm M_\odot}$ of stars formed, with a kinetic energy of $10^{51}\,{\rm erg}$ per supernova, would be sufficient to produce a kinetic energy density input from star formation of $4 \times 10^{-17}\,{\rm erg\,cm^{-3}}$, allowing for an efficiency of 1–10 per cent for the transferal of the kinetic energy of the supernovae to the IGM. So it is not implausible for feedback from galaxies in the form of supernova–driven winds to stir the IGM sufficiently to produce a significant in-

crease in the widths of the absorption lines. It is possible the presence of the narrow ($b < 15\,\mathrm{km\,s^{-1}}$) absorption systems detected in several of the QSO spectra, of which some if not all are due to metals, is evidence for supernovae feedback in the form of enriched material.

4.5 Gunn-Peterson effect

The original goal of searches for Lyα absorption in the spectra of QSOs was the discovery of intergalactic hydrogen, presumed to be uniformly distributed (Gunn & Peterson 1965). The discovery of a uniform component to the IGM has proven largely elusive, although searches continue. These are pursued under a variety of strategies: the search for additional Lyα absorption to what may be accounted for by Lyα forest blanketing alone (Steidel & Sargent 1987a), absorption in the spectra between Lyα forest absorption lines (Giallongo, Cristiani, & Trevese 1992), or determinations based on the distribution of pixel flux (Webb et al. 1992; Fang & Crotts 1995). The measurements provide additional constraints on the models presented here. The results of these measurements have generally placed an upper limit on the optical depth of a smooth component of 0.05–0.1, with a few claimed (but model-dependent) detections of this order, over the redshift range $2 < z < 5$.

The models discussed here show that essentially all the structure of the IGM is in the form of fluctuations that give rise to absorption features, even in underdense regions (Zhang et al. 1998), although a residual smooth component may be detectable in minivoids. A small amount of residual absorption may be reconciled with BBN constraints on Ω_b and a photoionizing background dominated by QSO sources, provided the systems giving rise to the Lyα forest have a characteristic line-of-sight scale length of $c_s/H(z) \approx L_J$, so that most of the baryons are contained in the Lyα forest (Meiksin & Madau 1993). This is explicitly demonstrated by the simulations. We may estimate the amount of additional absorption due to a smooth component as the difference $\tau_s = \bar{\tau}_\alpha - \tau_{\rm eff}$, where $\tau_{\rm eff}$ is the effective optical depth due to line-blanketing, given over a redshift interval Δz by $\tau_{\rm eff} = (1/\lambda_\alpha)\sum_i w_i^{\rm obs}/\Delta z$, where the sum is carried over the observed equivalent widths of the lines and λ_α is the (rest) wavelength of Lyα (Meiksin & Madau 1993; Press, Rybicki & Schneider 1993). The mean and effective optical depths measured from the spectra in Table 2 (with metal lines removed as discussed in Section 3) are shown in Figure 22. The differences in optical depth range over $0.01 < \tau_s < 0.05$. The predictions of the ΛCDM$_{\rm L}$ model are also shown. We find $\tau_s < 0.1$ at $z \simeq 3.5$, diminishing nearly to zero at lower redshift. Thus there is very little absorption present in both the measured and the model spectra that may not be accounted for by the Lyα forest alone. Similar results are found for the other models.

We also show in Figure 22 estimates for $\bar{\tau}_\alpha$ from Press, Rybicki & Schneider (1993) and Zhang et al. (1997), who based their estimates on the mean absorption measurements of Steidel & Sargent (1987b) and Zuo & Lu (1993). These measurements have been used in the past for estimating the amount of any residual optical depth after removing the effect of line-blanketing. The estimates of Press et al. (1993) lie systematically high, and those of Zuo & Lu (1993) lie systematically low, compared with the values we derive. Our values agree closely with those derived from the measurements of Steidel & Sargent (1987b), and with the recent determination by Kim, Cristiani & D'Odorico (2001). Adopting the values of Press et al. (1993) would in particular result in an overestimate of any residual optical depth beyond that due to line-blanketing.

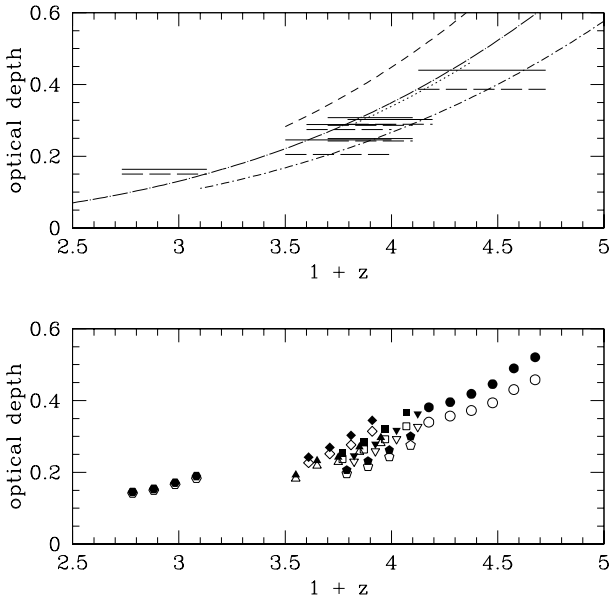

Figure 22. (Upper panel) Comparison between the total mean optical depth $\bar{\tau}_\alpha$ (solid bars) and the effective optical depth $\tau_{\rm eff}$ (long dashed bars) due to line-blanketing by the Lyα forest measured in the QSO spectra in Table 2. (The width of a bar indicates the redshift interval over which the optical depth is averaged.) Also shown are estimates for $\bar{\tau}_\alpha$ using data from Steidel & Sargent (1987b) (dotted line) and Zuo & Lu (1993) (dot-dashed line), the estimate of Press et al. (1993) (short dashed line), and the estimate of Kim et al. (2001) (dot-long dashed line). (Lower panel) The predictions of the ΛCDM$_{\rm L}$ model for $\bar{\tau}_\alpha$ (solid symbols) and $\tau_{\rm eff}$ (open symbols) for the spectra. The points near $z = 3$ have been slightly offset in redshift for clarity. The symbols correspond to Q1937−1009 (circles), HS 1946+7658 (triangles), Q0014+813 (inverted triangles), Q0302−003 (squares), Q0636+680 (diamonds), Q0956+122 (pentagons), J2233−606 (hexagons).

5 SUMMARY

We compare measurements of the Lyα forest in seven high resolution, high signal-to-noise ratio QSO spectra with predictions of hydrodynamical simulations for a variety of CDM dominated cosmologies. Spectra are synthesized from the simulations matching the observed spectra in wavelength coverage, pixelization, spectral resolution, and signal-to-noise properties. The statistical comparisons between the model and measured spectra are based on the distribution of flux per pixel and the statistics of the light fluctuations in the spectra as quantified by a wavelet analysis and by Voigt profile fitting to absorption features. Although all the models provide reasonably good qualitative descriptions of

the measured Lyα forest properties, we find varying levels of agreement with the data depending both on the cosmological model and the basis of comparison. In general, no single model is able to pass all the tests. The most accurate agreement is obtained for the flux per pixel distributions, with differences between the predicted and measured cumulative flux distributions as small as $d_{\rm KS} < 0.02$, close to the precision limit of the simulations and the measurements. Although the KS test formally rejects (at the 3σ level) almost all the predicted flux distributions in comparison with the measured, an analysis of the probability distribution of $d_{\rm KS}$ shows evidence for significant correlations in the flux values of neighbouring pixels. Allowing for the indicated reduction in the effective number of independent pixels results in acceptable fits provided by the ΛCDM and SCDM models, while the remaining models are strongly rejected. We find that the slope of the flux per pixel distribution systematically decreases with increasing $\sigma_{\rm J}$, the density fluctuations on the scale of the cosmological Jeans length. Agreement between the predicted and measured flux per pixel distributions imposes the restriction $1.3 < \sigma_{\rm J} < 1.7$ (better than 3σ), normalized at $z = 3$.

The predicted light fluctuations, as quantified by the wavelet analysis and fit absorption line parameters, are generally in poor agreement with the data. The most stringent statistical constraints are set by the distributions of wavelet coefficients, because of the large number of pixels available. (Correlations between the wavelet coefficients are weak or absent.) An advantage of the wavelet analysis over the more traditional Voigt profile analysis is that the orthogonality of the wavelets permits a separation of the velocity scales contaminated by metal lines from those dominated by Lyα absorption features. A further advantage is that it is extremely computationally cheap relative to a Voigt profile analysis, providing a very inexpensive means of testing model predictions for the statistics of the light fluctuations to high precision. The velocity range of approximately 15–30 $\rm km\,s^{-1}$ is of special interest since it corresponds to the velocity broadening of hydrogen absorption lines at the characteristic temperature of photoionized gas. Only the CHDM model is able to provide an acceptable match to the measured coefficients on this scale; all other models are strongly rejected. A conflict is thus presented in relation to the flux distribution: models that match well the measured flux per pixel distributions provide unacceptable matches to the wavelet coefficients, while those that are in agreement with the measured wavelet coefficients produce unacceptable pixel flux distributions. The agreement at smaller velocity scales is mixed, possibly due to contamination by metal absorption lines.

Voigt profile analyses are also performed, as they relate the light fluctuations to quantities of direct physical interest, the column densities and velocity widths of the absorption features. We find that while good agreement is often found between the predicted and measured $N_{\rm HI}$ distributions, including for models that produce satisfactory flux per pixel distributions, the agreement is mixed, depending on the analyis algorithm and the data. When agreement is found, it is often marginal. The agreement generally tends to favour the CHDM model, as for the wavelet coefficients. The same is true for the total number of absorption features. The models other than CHDM usually predict far too many absorption lines compared with the number measured in the spectra. The model predictions for the Doppler parameters fare much worse. The predicted median Doppler parameters are as much as 60 per cent smaller than the measured. As for the wavelet coefficients, the best agreement is generally provided by the CHDM model, although the predicted distributions are generally statistically unacceptable.

We find considerable inhomogeneity in the published data, particularly on the 15–30 $\rm km\,s^{-1}$ scale. Doppler parameter distributions independently derived from separate spectra covering nearly the same redshift range show statistically significant differences. This may lead to an exaggeration in the discrepancy between the Doppler widths found in simulations and the measured values appearing in some of the literature.

A breakdown of the absorption lines into subsamples optically thin and thick at the Lyα line centre shows that the discrepancies between the predicted and measured absorption line parameters originate primarily from the optically thin absorbers. The $N_{\rm HI}$ distributions predicted for the optically thick systems by most of the models are generally in good agreement with the measured distributions, as are the numbers of optically thick lines. Much poorer agreement is found for the $N_{\rm HI}$ distributions and line numbers for the optically thin absorbers. The Doppler parameters show a similar trend. The b-values of the optically thick absorbers are in much better accord with the data than those of the optically thin systems. The CHDM model again tends to provide the best agreement for both the b distributions and the total number of optically thin systems, as it did for the wavelet coefficients on the 16–32 $\rm km\,s^{-1}$ scale. This is no surprise, as all these distributions are related. The CHDM model produces broader features than the other models, so that fewer lines are required to reproduce the measured mean optical depth. The fewer lines are reflected by proportionally fewer large wavelet coefficients (fewer large light fluctuations), agreeing more closely with the measured coefficient distributions.

We consider a few possible explanations for the discrepant results for the light fluctuations. The most likely is perhaps late reionization of He II , at $z_{\rm HeII} \approx 3.5$. Late reionization will increase the temperature of the gas by an amount $\Delta T \approx 1.5 - 2 \times 10^4\,{\rm K}$. While the temperature of overdense gas will relax to lower values as a result of radiative losses, the lower density gas giving rise to the optically thin systems will retain a stronger memory of the boost in temperature, because it is too rarefied to radiate efficiently. We estimate the impact of the temperature boost for the $\Lambda{\rm CDM_L}$ model predictions for Q1937−1009 by convolving the simulation optical depths with a gaussian of velocity width $\sigma_T = 12\,\rm km\,s^{-1}$, corresponding to $\Delta T = 1.7 \times 10^4\,{\rm K}$. Excellent agreement is produced for the distributions of pixel flux, wavelet coefficients (on the 17–34 $\rm km\,s^{-1}$ scale), H I column density, and the median Doppler parameter. The extra broadening of the features has very little effect on the flux distribution, suggesting that the flux per pixel distribution provides a robust test of the models that is insensitive to uncertainties in the modelling of the reionization history of the IGM. We also consider the possible impact of galactic winds on the IGM and show that they too may plausibly provide sufficient broadening of the absorption features, provided they are able to propagate throughout the low density regions which give rise to the optically thin systems.

We caution against the use of any single distribution quantifying the light fluctuations, such as the wavelet coefficients, the H I column density, the Doppler parameters, or the number of absorption lines, as a test of the models. These quantities are all related, so that if a model fails to reproduce any one of them, whatever alterations to the model are necessary to gain accord with the data will disturb any agreement found in the remaining quantities.

The requirement that the models match the measured mean optical depths of the Lyα forest places a constraint on the H I photoionization rate. The models presented require an ionization rate that lies within a factor of 2 of that predicted for a UV background dominated by QSO sources. A large contribution from additional sources of ionizing radiation would place the models in jeopardy by requiring an implausibly high baryon density. We note, however, that the required photoionization background declines at $z > 3.1$ significantly more slowly than predicted by Haardt & Madau (1996) for a background dominated by QSO sources, based on current QSO counts. The mean optical depths obtained by the models are dominated by line-blanketing, with a residual optical depth resulting from a uniform component of at most 0.1 at $z \simeq 3.5$, and becoming vanishingly small by $z \simeq 2$.

Model	Ω_M	Ω_Λ	$\Omega_b h^2$	h	n	$\sigma_{8h^{-1}}$	$\sigma_{\rm J}$
CHDM	1	0	0.025	0.6	0.98	0.7	1.1
$\Lambda{\rm CDM_L}$	0.4	0.6	0.015	0.65	1	1.0	1.7
$\Lambda{\rm CDM_H}$	0.4	0.6	0.021	0.65	1	0.8	1.3
OCDM	0.4	0	0.015	0.65	1	1.0	2.2
SCDM	1	0	0.015	0.5	1	0.7	1.6
tCDM	1	0	0.025	0.6	0.81	0.5	0.9

Table 1. Parameters for the cosmological models. Ω_M is the total mass density parameter, Ω_Λ the cosmological constant density parameter, Ω_b the baryonic mass fraction, $h = H_0/100\,{\rm km\,s^{-1}\,Mpc^{-1}}$, where H_0 is the Hubble constant at $z = 0$, n the slope of the primordial density perturbation power spectrum, $\sigma_{8h^{-1}}$ the density fluctuation normalization in a sphere of radius $8h^{-1}$ Mpc, and $\sigma_{\rm J}$ the density fluctuation at $z = 3$ on the scale of the cosmological Jeans length (see text). For the CHDM model, two massive neutrino species are assumed accounting for a mass fraction of $\Omega_\nu = 0.2$.

QSO	$z_{\rm em}$	z range	pixel res	spectral res
Q1937−1009	3.806	3.126 − 3.726	7.4×10^4	9.0
HS 1946+7658	3.051	2.500 − 3.000	1.5×10^5	7.9
Q0014+813	3.384	2.794 − 3.194	0.06 Å	8.3
Q0302−003	3.286	2.700 − 3.100	0.06 Å	8.3
Q0636+680	3.174	2.600 − 3.000	0.06 Å	8.3
Q0956+122	3.301	2.700 − 3.100	0.06 Å	8.3
J2233−606	2.238	1.732 − 2.132	0.05 Å	6.7

Table 2. The QSO sample. The indicated redshift range is the portion of the spectrum adopted for the analysis. The pixel resolution (as $\lambda/\Delta\lambda$ or pixel width) and spectral resolution (FWHM in ${\rm km\,s^{-1}}$), correspond to this region. The observations were reported in: Q1937−1009: Burles & Tytler (1997); HS 1946+7658: Kirkman & Tytler (1997); Q0014+813, Q0302−003, Q0636+680, Q0956+122: Hu, Kim, Cowie & Songaila (1995); J2233−606: Cristiani & D'Odorico (2000).

ACKNOWLEDGMENTS

This work is supported in part by the NSF under the auspices of the Grand Challenge Cosmology Consortium (GC^3). The computations were performed on the Convex C3880, the SGI Power Challenge, and the Thinking Machines CM5 at the National Center for Supercomputing Applications, and the Cray C90 at the Pittsburgh Supercomputing Center under grant AST950004P. AM thanks S. Burles and D. Tytler for providing an unpublished electronic version of the spectrum of Q1937−1009, and R. Davé for permission to use AutoVP. Support for GLB was provided by NASA through Hubble Fellowship grant HF-01104.01-98A from the Space Telescope Science Institute, which is operated by the Association of Universities for Research in Astronomy, Inc., under NASA contract NAS6-26555. MM would like to acknowledge the hospitality of the MIT astrophysics group.

APPENDIX A: TESTS OF ANALYSIS PROCEDURES

In this section we summarise several tests of the analysis procedures: the redshift interpolation method, the noise models, the goodness-of-fit of the absorption line analyses, and the applicability of the KS test.

A1 Redshift interpolation

We test the redshift interpolation method using the distributions found in the $\Lambda{\rm CDM_H}$ simulation. In Figure A1, the effect of rescaling the flux distributions at $z = 3$ and $z = 4$ to redshifts $z = 4$ and $z = 3$, respectively, is shown using the values for α in Table 3 and equation 1. (No additional evolution in the radiation field was assumed: $p = 0$.) The result of rescaling the spectra at $z = 3$ and $z = 4$ both to $z = 3.6$ and then linearly weighting the resulting flux distributions to $z = 3.6$ using equation 2 is shown by the central dashed curve. The difference between the direct and interpolated cumulative distributions at $z = 3.6$ is at most 0.006, and indicates the level of accuracy of the modelling of the measured spectra. A similar level of accuracy is found for the cumulative distributions of the wavelet coefficients. The direct and interpolated distributions of the absorption line parameters, however, agree somewhat more poorly. While the cumulative distributions generally agree to within a difference of 0.01, portions may disagree by as much as 0.03 for the $N_{\rm HI}$ distribution and 0.04 for the b distribution at intermediate values, in the sense that the interpolated distributions exceed the directly estimated distributions. These differences are comparable to the accuracy to which the distributions may be measured using a single QSO spectrum and represent a limitation of the modelling of the distributions. Since it was based on a near maximum amount of interpolation to an intermediate redshift between the data dump redshifts, we expect that the actual modelling is some-

Model	α	p	ω	s
CHDM	6.3	0.0	0	0.3274
CHDM	6.3	5.0	0	0.5525
CHDM	6.3	5.0	0.04	0.63
ΛCDM$_{\rm L}$	7.4	0.0	0	1.465
ΛCDM$_{\rm L}$	7.4	5.0	0	2.443
ΛCDM$_{\rm L}$	7.4	5.0	0.013	2.56
ΛCDM$_{\rm H}$	6.8	0.0	0	0.5218
ΛCDM$_{\rm H}$	6.8	5.0	0	0.8783
ΛCDM$_{\rm H}$	6.8	5.0	0.022	0.94
OCDM	7.4	0.0	0	3.119
OCDM	7.4	4.5	0	4.937
OCDM	7.4	4.5	0.005	4.937
SCDM	7.0	0.0	0	1.291
SCDM	7.0	5.0	0	2.105
SCDM	7.0	5.0	0.018	2.3
tCDM	6.4	0.0	0	0.3076
tCDM	6.4	5.2	0	0.5260
tCDM	6.4	5.2	0.056	0.63

Table 3. Evolution exponents, continuum offsets, and rescaling coefficients for the predicted distributions of flux per pixel to match that measured in Q1937−1009. The value for α corresponds to the redshift interval $3 < z < 4$.

Model	α	ω	s
CHDM	6.3	0.03	0.59
ΛCDM$_{\rm L}$	6.8	0.005	2.1
ΛCDM$_{\rm H}$	6.8	0.015	0.85
tCDM	6.4	0.04	0.59

Table 4. Evolution exponents, continuum offsets, and rescaling coefficients for the predicted distributions of flux per pixel to match that measured in HS 1946+7658. The value for α corresponds to the redshift interval $2 < z < 3$.

what better. Nevertheless, in the future a greater number of intermediate data dump redshifts would be desirable.

A2 Absorption line goodness-of-fit

Because of the necessarily automated nature of the absorption line parameter analyses, it is important to maintain a check on the acceptability of the fits. This was done by tabulating the distributions of χ^2 for the fit line complexes for all of the analyses. Because the number of degrees-of-freedom $n_{\rm dof}$ differs for different line complexes, the quantity tabulated is $(\chi^2/n_{\rm dof}-1)/(2/n_{\rm dof})^{1/2}$, which in the limit $n_{\rm dof}\rightarrow\infty$ is distributed like a gaussian with zero mean and unit variance (Kendall & Stuart 1969). The resulting cumulative distributions for the ΛCDM$_{\rm L}$ model predictions for Q1937−1009 (assuming no continuum offset) are shown for AutoVP and SPECFIT in Figure A2, which are representative of all the analyses. The fits are generally acceptable, although both line analysis methods produce a tail of high χ^2 values. The low median value of χ^2 produced by AutoVP is a consequence of the demand for a reduced χ^2 of 0.5 for a fit to be acceptable. For SPECFIT, the requirement was a reduced χ^2 of 1.

Model	ω	s
Q0014+813		
CHDM	0.08	0.6263
ΛCDM$_{\rm L}$	0.03	2.2
ΛCDM$_{\rm H}$	0.05	0.90
tCDM	0.08	0.60
Q0302−003		
CHDM	0.075	0.74
ΛCDM$_{\rm L}$	0.03	2.7
ΛCDM$_{\rm H}$	0.05	1.09
tCDM	0.08	0.72
Q0636+680		
CHDM	0.075	0.82
ΛCDM$_{\rm L}$	0.026	2.90
ΛCDM$_{\rm H}$	0.045	1.15
tCDM	0.08	0.80
Q0956+122		
CHDM	0.06	0.54
ΛCDM$_{\rm L}$	0.025	1.88
ΛCDM$_{\rm H}$	0.045	0.81
tCDM	0.08	0.57
J2233−606		
CHDM	0.06	1.3
ΛCDM$_{\rm L}$	0.024	4.5
ΛCDM$_{\rm H}$	0.04	1.95
tCDM	0.06	1.25

Table 5. Continuum offsets and rescaling coefficients for the predicted distributions of flux per pixel to match those measured in Q0014+813, Q0302−003, Q0636+680, Q0956+122, and J2233−606.

A3 KS test

The acceptability of a hypothesis using the KS test is determined by the probability of exceeding the value $N^{1/2}d_{\rm KS}$, where $d_{\rm KS}$ is the maximum difference (in absolute value) between the cumulative distribution of some parameter measured independently N times, and the predicted distribution. The probability distribution for exceeding $N^{1/2}d_{\rm KS}$ in the flux per pixel distribution derived from the simulated spectra of the ΛCDM$_{\rm L}$ model (with no continuum offset), using as the fiducial the average distribution of flux per pixel predicted for Q1937−1009, is shown in Figure A3. The distribution of $N^{1/2}d_{\rm KS}$ derived from the simulated spectra is broader than the theoretical KS probability distribution. Also shown are the probability distributions of $N^{1/2}d_{\rm KS}$ based on the distributions of $N_{\rm HI}$ and b from the AutoVP analysis. In contrast to the case for the flux, these distributions are much narrower than the theoretical distribution.

The reasons for the discrepancies in the distributions are unclear. Since absorption features typically run over several pixels, individual pixel fluxes will not be statistically independent, as is required for the validity of the KS test. Similarly, since the absorption line analysis procedure fits nearby lines simultaneously, the values found for the fit parameters are not truly independent.

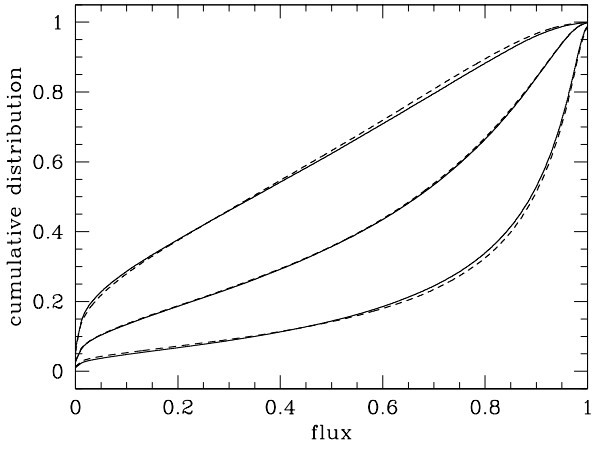

Figure A1. Test of the interpolation method for the flux distribution, for the ΛCDM$_{\rm H}$ model. The left pair of curves show the flux distribution at $z = 4$ (solid curve) and the predicted distribution based on rescaling the model spectra at $z = 3$ according to equation 1 (dashed curve). The right pair of curves show the flux distribution at $z = 3$ (solid curve) and the predicted distribution from rescaling the spectra at $z = 4$ (dashed curve). The central pair show the flux distribution at $z = 3.6$ (solid curve) and the linearly interpolated distribution based on rescaling the spectra at $z = 3$ and $z = 4$ and using equation 2 (dashed curve). The predicted and actual distributions at $z = 3.6$ agree to within 0.4 per cent.

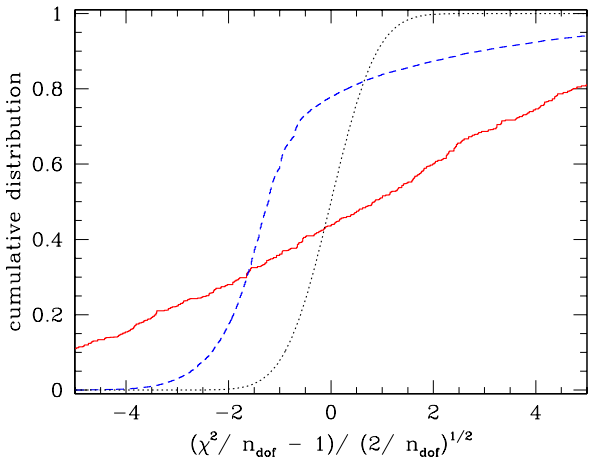

Figure A2. Distribution of χ^2 for the absorption line fits using AutoVP (solid curve) and SPECFIT (dashed curve), for ΛCDM$_{\rm L}$. Shown are the cumulative distributions of $(\chi^2/n_{\rm dof} - 1)/(2/n_{\rm dof})^{1/2}$, where $n_{\rm dof}$ is the number of degrees-of-freedom of the fit. This quantity should be distributed like a gaussian with vanishing mean and unit variance in the limit $n_{\rm dof} \rightarrow \infty$ (dotted curve). Although most of the fits are acceptable, both methods produce too great a tail at large χ^2 values.

We examine the possible effect of correlations in flux and in the derived absorption parameter values using a set of Monte Carlo simulations of spectra. We model the statistical distribution of the line positions, H I column densities, and Doppler parameters based on the distributions reported in Kirkman & Tytler (1997) (see Appendix B below). The resulting probability distribution of $N^{1/2}d_{\rm KS}$ for the flux, shown in Figure A3, is again found to be broader than the KS distribution, and even broader than the distribution derived from the simulation. This suggests that strong correlations in the pixel fluxes are present. Allowing for a reduction by a factor of 3 in the effective number of independent flux measurements shifts the theoretical KS probability distribution into good agreement with that derived from the simulation, while a reduction by a factor of 5 produces good agreement between the theoretical probability distribution and that measured from the Monte Carlo realizations. The resulting probability distributions of $N^{1/2}d_{\rm KS}$ based on the derived values of $N_{\rm HI}$ and b using AutoVP are found to be narrower than the KS distribution, although not by as much as the simulation results. Once again, correlations appear to be present, but tending to reduce the scatter in the derived values of the absorption line parameters.

An element of statistical dependence in the simulation results may also arise because the lines-of-sight sampled in the simulation are not truly statistically independent since they are drawn from the same simulation, and so may give a biased estimate of the correct distribution function with a reduced dispersion. This may only be tested using lines-of-sight that are spaced adequately to probe separate structures, or by a large number of repeated simulations. Neither is currently computationally feasible using full hydrodynamical simulations, so that this possibility cannot be tested at present.

Still another possibility is that the properties of nearby features are physically related. Such correlations are expected for neighbouring lines–of–sight as a consequence of the linear continuity of the gas density defining the filaments. Similar correlations may exist among density fluctuations across the filaments. In this paper, we quote formal KS probabilities, noting that these appear to underestimate the true probabilities for the flux distribution comparisons and to be conservative estimates of the probabilities for the comparisons of the absorption line parameter values. Possibly more realistic estimates of the flux per pixel distribution KS-test probabilities are provided by reducing the effective number of pixels by a factor of 3–5, and so these values are also quoted.

APPENDIX B: COMPARISON OF AutoVP AND SPECFIT

In this Appendix, the line finding and fitting algorithms used in this paper, AutoVP and SPECFIT, are compared using

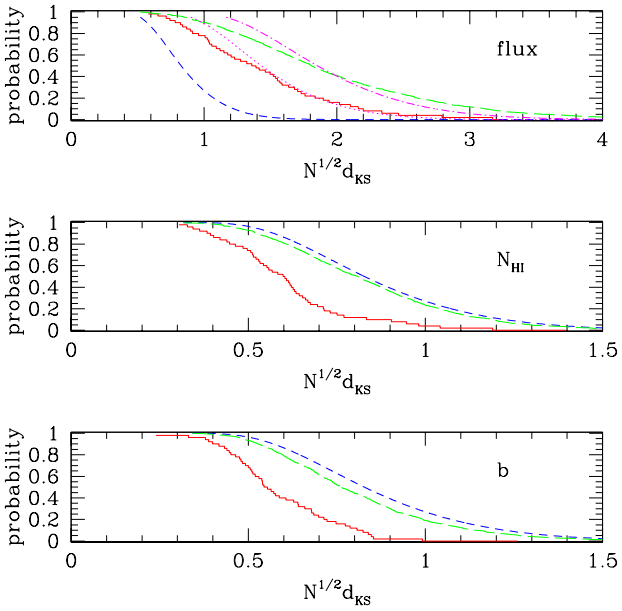

Figure A3. Test of the distribution of probability of exceeding a given value of $N^{1/2}d_{\rm KS}$, where $d_{\rm KS}$ is the maximum difference between the cumulative distribution of N values of flux (top panel), $N_{\rm HI}$ (middle panel), and b (bottom panel), and the expected distributions, using the predictions of the $\Lambda{\rm CDM_L}$ model for Q1937−1009. The probability distribution derived from the simulation (solid histograms) is broader for the flux, and narrower for the absorption line parameters, than the respective KS probability distributions (short dashed curves). The distributions for a set of Monte Carlo realisations of the Lyα forest are also shown (long dashed curves). Also shown in the top panel are the KS probability curves assuming a reduction in the effective number of independent pixels by a factor of 3 (dotted curve) and 5 (dash-dotted curve).

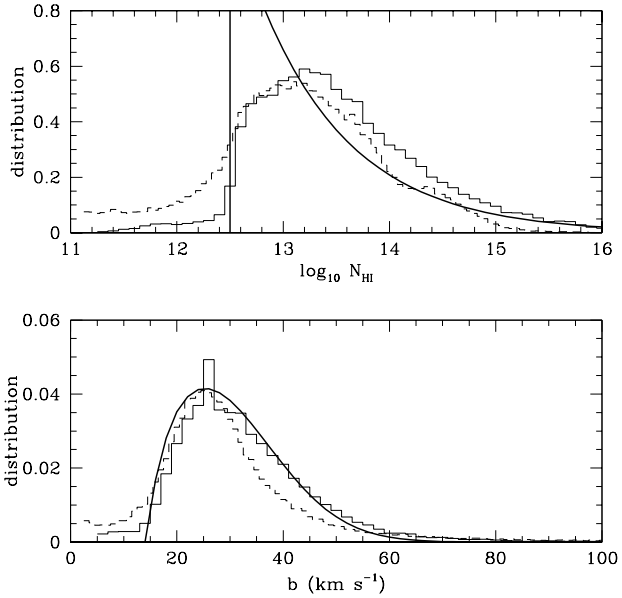

Figure B1. The recovered H I column density and Doppler parameter distributions from a set of Monte Carlo realizations. The light solid curves show the results of AutoVP while the dashed curves show the results of SPECFIT. The heavy solid lines show the input model distributions.

Monte Carlo realisations of spectra. The algorithm for AutoVP is described by Davé et al. (1997). SPECFIT performs its analysis through the following steps: 1. filter the spectrum using wavelets, discarding the smallest wavelet coefficients to ensure a reduced χ^2 of 1 between the filtered and unfiltered spectrum; 2. identify candidate features as inflection points by computing a smoothed second derivative of the spectrum; 3. define a spectral region to be fit about each candidate line as a contiguous region with the flux smaller than a given $\exp(-\tau_{\rm min})$; 4. merge overlapping regions into single regions, provided the number of candidates in a single region is not too great, in which case it is split (at most 16 candidate lines were allowed in a single fit region in the analyses of this paper); 5. perform a non-linear least squares fit of the candidate lines to the original (unfiltered) spectrum.

The spectra are constructed from discrete lines with Voigt profiles using the H I column density and Doppler parameter distributions found by Kirkman & Tytler (1997). Specifically, the H I column densities $N_{\rm HI}$ are drawn independently from a power law distribution of slope 1.5 between $12.5 < \log_{10} N_{\rm HI} < 16$ and the Doppler parameters b from a gaussian with mean 23 $\rm km\,s^{-1}$ and standard deviation 14 $\rm km\,s^{-1}$. A cut–off in b is imposed according to $b > 14 + 4(\log_{10} N_{\rm HI} - 12.5)$ $\rm km\,s^{-1}$. The resulting average Doppler parameter is 31 $\rm km\,s^{-1}$. The number density of lines per unit redshift matches that of Kirkman & Tytler (1997) at $z = 3$. The resolution is set at $\lambda/d\lambda = 5\times10^4$, and gaussian noise is added to give a continuum signal–to–noise ratio per pixel of 50.

The two methods are found to have relative advantages and disadvantages. AutoVP faithfully recovers the cut-off in the H I column density distribution at $\log_{10} N_{\rm HI} = 12.5$, while SPECFIT produces an excess of low column density systems. At higher column densities ($13 < \log_{10} N_{\rm HI} < 15$), however, SPECFIT is found to better recover the input column density distribution.

By contrast, AutoVP well reproduces the input Doppler parameter distribution, although it produces a small tail at low values. SPECFIT similarly produces a low b tail, and somewhat underpredicts the number of intermediate b systems.

It is evident that neither algorithm perfectly recovers the input parameter distributions. No improvement in the signal–to–noise ratio would yield better results: the discrepancy arrises from the unavoidable blending of features. In practice, provided the same algorithm is applied to the data and the model spectra, the resulting fits may still be used as a viable statistical description of the light fluctuations in the spectra.

REFERENCES

Abel T., Haehnelt M., 1999, ApJ, 520, L13
Aguirre A., Hernquist L., Schaye J., Weinberg D. H., Katz N., Gardner J., 2001, preprint (astro-ph/0006345)

Bardeen J. M., Bond J. R., Kaiser N., Szalay A. S., 1986, ApJ, 304, 15
Bertschinger E., 1995, preprint (astro-ph/9506070)
Boksenberg A., Sargent W. L. W., Rauch M., 1998, preprint (astro-ph/9810502)
Bond J. R., Myers, S. T., 1996, ApJS, 103, 63
Bond J. R., Wadsley J. W., 1997, in Petitjean P., Charlot S., eds, Structure and Evolution of the Intergalactic Medium from QSO Absorption Line Systems. Editions Frontières, Paris, p. 143
Bryan G. L., Machacek M. E., 2000, ApJ, 534, 57
Bryan G. L., Machacek M., Anninos P., Norman M. L., 1999, ApJ, 517, 13
Bryan G. L., Norman M. L., Stone J. M., Cen R., Ostriker J. P., 1995, Comput. Phys. Commun., 89, 149
Bunn E F., White M., 1997, ApJ, 480, 6
Burles S., Tytler D., 1997, AJ, 114, 1330
Burles S., Tytler D., 1998, ApJ, 499, 699
Cen R., Miralda-Escudé J., Ostriker J. P., Rauch M., 1994, ApJ, 437, L9
Copi C. J., Schramm D. N., Turner M. S., 1995, ApJ, 455, L95
Cristiani S., D'Odorico V., 2000, AJ, 120, 1648
Croft R. A. C., Weinberg D. H., Bolte M., Burles S., Hernquist L., Katz N., Kirkman D., Tytler D., 2000, preprint (astro-ph/0012324)
Croft R. A. C., Weinberg D. H., Katz N., Hernquist L., 1997, ApJ, 488, 532
Davé R., Hernquist L., Weinberg D. H., Katz N., 1997, ApJ, 477, 21
Eke V. R., Cole S., Frenk C. S., 1996, MNRAS, 282, 263
Eisenstein D. J., Hu W., 1999, ApJ, 511, 5
Eisenstein D. J., Zaldarriaga M., 2001, ApJ, 546, 2
Fang Y., Crotts P. S., 1995, ApJ, 440, 69
Ferrara A., Pettini M., Shchekinov Y., 2000, MNRAS, 319, 539
Giallongo E., Cristiani S., Trevese T., 1992, ApJ, 398, L9
Gnedin N. Y., 1998, MNRAS, 299, 392
Gunn J. E., Peterson B. A., 1965, ApJ, 142, 1633
Haardt F., Madau P., 1996, ApJ, 461, 20
Haehnelt M. G., Steinmetz M., 1998, MNRAS, 298, L21
Hernquist L., Katz N., Weinberg D., Miralda-Escudé J., 1996, ApJ, 457, L51
Hu E. M., Kim T. S., Cowie L. L., Songaila A., Rauch M., 1995, AJ, 110, 1526
Hui L., Gnedin N. Y., 1997, MNRAS, 292, 27
Izotov Y. I., Thuan T. X., 1998, ApJ, 500, 188
Kendall M. G., Stuart A., 1969, The Advanced Theory of Statistics, vol. 1. Charles Griffin & Co., London
Kim T.-S., Cristiani S., D'Odorico S., 2001, A&A (in press) (astro-ph/0101005)
Kim T.-S., Hu E. M., Cowie L. L., Songaila A., 1997, AJ, 114, 1
Kirkman D., Tytler D., 1997, ApJ, 484, 672
Lu L., Sargent W. L. W., Womble D. S., Takada-Hidai M., 1996, ApJ, 472, 509
McDonald P., Miralda-Escudè J., Rauch M., Sargent W. L. W., Barlow T. A., Cen R., 2000a, preprint (astro-ph/0005553)
McDonald P., Miralda-Escudè J., Rauch M., Sargent W. L. W., Barlow T. A., Cen R., Ostriker J. P., 2000b, ApJ, 543, 1
Machacek M. E., Bryan G. L., Meiksin A., Anninos P., Thayer D., Norman M. L., Zhang Y., 2000, ApJ, 532, 118 (M00)
Madau P., Efstathiou G., 1999, ApJ, 517, L9
Madau P., Ferguson H. C., Dickinson M. E., Giavalisco M., Steidel C. C., Fruchter A., 1996, MNRAS, 283, 1388
Madau P., Ferrara A., Rees M. J., 2000, preprint (astro-ph/0010158)
Madau P., Meiksin A., 1994, ApJ, 433, L53
Meiksin A., 1994, ApJ, 431, 109
Meiksin A., 2000, MNRAS, 314, 566
Meiksin A., Madau P., 1993, ApJ, 412, 34
Meiksin A., White M., 2001, MNRAS, 324, 141
Miralda-Escudé J., Cen R., Ostriker J. P., Rauch M., 1996, ApJ, 471, 582
Miralda-Escudé J., Rees M. J., 1994, MNRAS, 266, 343
Nath B. B., Trentham N., 1997, MNRAS, 291, 505
Netterfield C. B., et al. , 2001, preprint (astro-ph/0104460)
O'Meara J. M., Tytler D., Kirkman D., Suzuki N., Prochaska J. X., Lubin D., Wolfe A. M., 2000, preprint (astro-ph/0011179)
Peebles P. J.P., 1984, ApJ, 277, 470
Peebles P. J. P., 1993, Principles of Physical Cosmology. Princeton University Press, Princeton
Pierpaoli E., Scott S., White M., 2001, preprint (astro-ph/0010039)
Press W. H., Rybicki G. B., Schneider D. P., 1993, ApJ, 414, 64
Pryke C. et al. , 2001, preprint (astro-ph/0104490)
Rauch M. et al. , 1997, ApJ, 489, 7
Reimers D., Köhler S., Wisotzki L., Groote D., Rodriguez-Pascual P., Wamsteker W., 1997, A&A, 327, 890
Rhoads J. E., Malhotra S., Dey A., Jannuzi B. T., Stern D., Spinrad H., 2001, in Clowes R. G., ed, ASP Conf. Ser., The New Era of Wide-Field Astronomy. APS, San Francisco, in press
Ricotti M., Gnedin N. Y., Shull J. M., 2000, ApJ, 534, 41
Schaye J., Theuns T., Rauch M., Efstathiou G., Sargent W. L. W., 2000, MNRAS, 318, 817
Seljak U., Zaldarriaga M., 1996, ApJ, 469, 437
Songaila A., Cowie L., 1996, AJ, 112, 335
Steidel C. C., Adelberger K. L., Giavalisco M., Dickinson M., Pettini M., 1999, ApJ, 519, 1
Steidel C. C., Sargent W. L. W., 1987a, ApJ, 318, L11
Steidel C. C., Sargent W. L. W., 1987b, ApJ, 313, 171
Stompor R. et al. , 2001, preprint (astro-ph/0105062)
Theuns T., Leonard A., Efstathiou G., 1998a, MNRAS, 297, L49
Theuns T., Leonard A., Efstathiou G., Pearce F. R., Thomas P. A., 1998b, MNRAS, 301, 478
Theuns T., Leonard A., Schaye J.,Efstathiou G., 1999, MNRAS, 303, L58
Theuns T., Mo H. J., Schaye J., 2001, MNRAS, 321, 450
Theuns T., Schaye J., Haehnelt M. G., 2000, MNRAS, 315, 600
Wang B., 1995, ApJ, 444, 590
Webb J. K., Barcons X., Carswell R. F., Parnell H. C., 1992, MNRAS, 255, 319
Weinberg D. H., et al. , 1999, Banday A. J., Sheth R. K., Da Costa L. N., eds, Evolution of Large Scale Structure: From Recombination to Garching. Twin Press, Vledder, p. 346
Weinberg D. H., Miralda-Escudé J., Hernquist L., Katz N., 1997, ApJ, 490, 564
White S. D. M., Efstathiou G., Frenk C. S., 1993, MNRAS, 262, 1023
Zhang Y., Anninos P., Norman M. L., 1995, ApJ, 453, L57
Zhang Y., Anninos P., Norman M. L., Meiksin A., 1997, ApJ, 485, 496
Zhang Y., Meiksin A., Anninos P., Norman M. L., 1998, ApJ, 495, 63
Zuo L., Lu L., 1993, ApJ, 418, 601
Zuo L., Bond J. R., 1994, ApJ, 423, 73